Monitoring and Modeling Part Thickness in Vacuum Assisted Resin Transfer Molding

by

Nazlı Köroğlu

A Dissertation Submitted to the
Graduate School of Sciences and Engineering
in Partial Fulfillment of the Requirements for
the Degree of

Master of Science

in

Mechanical Engineering

September 22, 2020

Monitoring and Modeling Part Thickness in Vacuum Assisted Resin Transfer Molding

Koç University

Graduate School of Sciences and Engineering

This is to certify that I have examined this copy of a master's thesis by

Nazlı Köroğlu

and have found that it is complete and satisfactory in all respects,
and that any and all revisions required by the final
examining committee have been made.

Committee Members:

_____

Prof. E. MURAT SÖZER (Advisor)

_____

Prof. DEMİRCAN CANADİNÇ

_____

Assist. Prof. ERALP DEMİR

Date: 22.09.2020

ABSTRACT

Monitoring and Modeling Part Thickness in Vacuum Assisted Resin Transfer Molding

Nazlı Köroğlu

Master of Science in Mechanical Engineering

September 22, 2020

This thesis successfully uses Structured Light Scanning (SLS) to monitor a composite part's thickness distribution as it is being manufactured with Vacuum Assisted Resin Transfer Molding (VARTM). As resin is infused through a porous fabric preform, local resin pressure and thus compaction pressure acting on the preform change causing thickness to vary spatially and with time. Integration of SLS system with a VARTM setup also allows to conduct compaction characterization of fabric preforms. SLS full-field thickness monitoring allows to record statistical variations and thus superior to instruments such as dial gages which measure thickness at a point only.

After the mold is filled with resin, the injection gates are closed, and vacuuming is continued through the ventilation ports to see the effect of resin bleeding. This action evacuates excess resin out and settles pressure with time. Thickness decreases from 1.72+/-0.27 mm just before closing the inlet to 1.55+/-0.17 mm 300 s later in 2D experiment. Corresponding fiber volume fraction increases from 0.19+/-0.03 to 0.21+/-0.02, thickness variation decreases from 2.32 to 1.55 mm, respectively. Resin pressure and part thickness are modeled and compared with the experimental data in 2D resin flow case. Resin pressure is solved by discretizing continuity equation (Darcy velocity components substituted in mass conservation equation) using Finite Difference Method. At the steady state, the difference between simulated and experimental flow rates through inlet is 0.5% showing that the material characterization, flow and compaction modeling are useful tools to predict resin flow as well as part thickness distribution.

ÖZETÇE

Vakum Destekli Reçine Transfer Kalıplama (VARTM) Yönteminde Parça Kalınlığının İzlenmesi ve Modellenmesi

Nazlı Köroğlu

Makine Mühendisliği, Yüksek Lisans

22 Eylül 2020

Vakum Destekli Reçine Transfer Kalıplama (VARTM) yöntemi ile üretilen kompozit malzemenin kalınlık dağılım ölçümü Yapısal Aydınlatma ile Tarama (*Structured Light Scanning (SLS)*) yöntemiyle yapıldı. Reçinenin elyaf yatağına infüzyonuyla, konumsal reçine basıncı değişir; bundan dolayı sıkıştırma basıncının değişmesiyle, malzeme kalınlığı pozisyona ve zamana bağlı olarak değişmektedir. VARTM düzeneği ile SLS sisteminin birlikte kullanılması elyaf yatağının sıkıştırma karakterizasyonunun ve parça kalınlık dağılımının ölçülmesine olanak sağlamıştır. Tüm parçaların SLS ile kalınlık ölçümü, istatistiksel farklılıkları kaydedebildiği için, komparatör gibi sadece tek noktada ölçüm yapabilen diğer alternatif aletlere göre daha üstündür.

Kalıp içindeki fazlalık reçinenin tahliye edilmesi (*resin bleeding*) etkisini gözlemleyebilmek için, kalıp reçine ile tamamen dolduktan ve elyaf yatağı doyduktan sonra, reçine girişi kapatılmış ve çıkış vanasından vakumlamaya devam edilmiştir. Bu aksiyon, fazlalık reçinenin tahliye edilmesini ve basınç dağılımının zamanla dengeye ulaşmasına yardımcı olmuştur. İki boyutlu akış deneyinde, kalınlık 1.72+/-0.27 mm'den (giriş vanasını kapatmadan hemen önce) 1.55+/-0.17 mm'ye (300 saniye sonra) düşmüştür. Bu değerlere karşılık gelen hacimsel lif oranları (*fiber volume fraction*) 0.19+/-0.03'ten 0.21+/-0.02'ye artmıştır. Tüm parça içinde kalınlık varyasyonu da 2.32 mm'den 1.55 mm'ye düşmüştür. Reçine basıncı ve parça kalınlığı modellenmiş ve deneysel iki boyutlu akış verisiyle kıyaslanmıştır. Kütlenin korunumu denklemi (içinde Darcy kanununun hız bileşenleri kullanılarak), Sonlu Farklar Yöntemi (FDM) ile çözülerek reçine basıncı sayısal olarak elde edilmiştir. Kararlı durumda, giriş kısmındaki hacimsel akış debisinin model ve deneysel değerleri arasındaki fark %0.5 olarak hesaplanmıştır. Bu durum malzeme karakterizasyonu, akış ve sıkıştırma modellemesinin, reçine akışı ve parça kalınlık dağılımının önceden tahmin edilmesi için yararlı olduğunu göstermiştir.

AKNOWLEDGEMENTS

I would like to thank my advisor Prof. E. Murat Sözer for his support, patience, and guidance at every stage of my graduate study. I would like to thank members of my thesis committee Prof. Demircan Canadinç and Assist. Prof. Eralp Demir for their participation with insightful comments.

I would also like to thank to the staff of Graduate School of Sciences and Engineering and College of Engineering for their support and patience.

I would also like to thank to my colleagues Hasan Çağlar and Mert Hancıoğlu in Composite Materials Manufacturing Laboratory for their support in laboratory studies and friendship. Also, I would like to thank Barış Çağlar, Berke Öznalbant and Serhan Enes Kalmış for their help during my experiments.

I am thankful to 8/F + OOS for their supportive friendship since 2003. Especially, Ahmet Çam, Dila Civanbay, Oğuz Torunoğlu. Also, thanks to Mine Özataş, Zeynep Boran Yel, Özge Odabaşı for their friendship, and support.

Finally, I would like to give my biggest thank to my family, my mother Nahide Köroğlu, my father Avni Köroğlu and my sister İpek Köroğlu for their endless love, support, and patience during my whole life.

TABLE OF CONTENTS

LIST OF TABLES

LIST OF FIGURES

ABBREVIATIONS

FRPC	Fiber Reinforced Plastic Composites
LCM	Liquid Composite Molding
RTM	Resin Transfer Molding
VARTM	Vacuum Assisted Resin Transfer Molding
SLS	Structured Light Scanning
P_c	Compaction pressure
P_r	Resin pressure
P_{atm}	Atmospheric pressure
h	Thickness
V_f	Fiber Volume Fraction
K_{uns}	Unsaturated permeability
K_s	Saturated permeability
n	Number of layers
ρ_{sup}	Superficial density
ρ_f	Polypropylene (bulk) density
ϕ	Porosity
μ	Viscosity
t_{fill}	Filling time

Chapter 1:
INTRODUCTION

Composites consist of at least two distinct materials which have different chemical or physical properties. Their combination creates more convenient and different characteristics from individual constituents. Fiber reinforced plastic composites (FRPC) are one of the most commonly used composites type in aerospace, automotive, infrastructure, defense and sportive good industries. The two components of FRPC include a polymeric resin (matrix component) and a reinforcement material (usually a fiber preform); they are combined and consolidated to form the composite. A liquid polymeric resin (matrix phase of the composite) impregnates empty spaces (porous parts) of a fiber preform and has the following roles: (i) preserve fiber structure and orientation after it cures, (ii) dissipates a load to the fiber network, (iii) protects fibers from environmental conditions like humidity and sunlight. The polymeric resin can be either thermoplastic or thermoset. However, thermosets are usually used in Liquid Composite Molding (LCM) manufacturing processes because of their low viscosity when compared to thermoplastics. Low viscosity allows filling empty spaces between continuous fibers. A preform structure of fibers (usually in the form of cut and stacked layers of a fabric which is made of fiber bundles) is the reinforcement component of the composites which is placed in the mold cavity before the resin injection. Fibers could be glass, carbon, or Kevlar. Fibers support major fraction of structural load (which is acting on a composite structure) and provide stiffness to the composite, whereas matrix cured thermoset polymer gives the shape to flexible fibers and protects the fibers from the environmental effects [1].

Manufacturing of composite materials is very different from manufacturing of traditional materials like metals or ceramics. Composites replace traditional materials over time. Composites have been used in a wide range of industries from aerospace to renewable energy. Composite materials have some advantages and disadvantages when compared to traditional materials. Fiber reinforced plastic composites have high strength-to-weight ratio which is crucial in aerospace and automotive industries because of fuel economy. Carbon fiber composites are 50% lighter than steel [2] which decreases vehicle weight when composites are used, also crash safety improves because multilayer composite laminates can absorb more impact energy than traditional single-layer steel

[17]. Composites are more durable, and their corrosion resistance property makes them preferable in the marine industry and these benefits reduce maintenance costs. Composites offer design robustness compared to assembled metal parts. For instance, lower half of a boat hull can be manufactured as a single composite part. On the other hand, manufacturing processes of composite materials have some disadvantages and limitations. One of the major issues is that manufacturing of parts is not repeatable (i.e. dimensional and mechanical properties may vary significantly among parts) and not totally standardized when compared to metals. Irregularities and deformations in fabric rolls during storage and handling cause variations in tows (fiber bundles) such as irregular orientation, waviness, and misalignment (uneven spacing). In addition to these, labor of fabric cutting, stacking, and placement of the fabric preform into a mold cavity may differ among workers. These effects can change the properties of composites adversely (permeability of the fiber preform during resin injection; dimensional tolerances, physical and mechanical properties of the final part).

1.1 Liquid Composite Molding (LCM) Processes

LCM processes are a sort of composite material manufacturing methods. In these processes, a dry reinforcement material (stacked fabric layers of continuous or discontinuous fibers made from glass, carbon, or Kevlar) is placed in the mold cavity and then impregnated with a polymeric resin. Some of the major LCM processes are Resin Transfer Molding (RTM), Vacuum Assisted Resin Transfer Molding (VARTM), Seeman's Composite Resin Infusion Molding Process (SCRIMP), Structural Reaction Injection Molding (S-RIM), Co-Injection Resin Transfer Molding (CIRTM) and so on [1]. RTM and VARTM (a.k.a. Vacuum Infusion, VI) are the most common LCM processes [1].

1.1.1 Resin Transfer Molding (RTM)

In RTM, there are at least two semi-rigid matched mold parts which can be made from aluminum, steel, or fiber reinforced plastic composites. The mold is a two-sided type and it has a cavity in the shape of manufactured part. Fabric preform is placed in that cavity, and the mold is closed by using clamps or a press. Empty spaces between fibers are filled by a thermoset resin under positive pressure by using an injection machine [3]. Thickness and permeability do not change with time as the mold parts are semi-rigid and

thus fiber volume fraction is constant. Figure 1.1 demonstrates the steps of the RTM process.

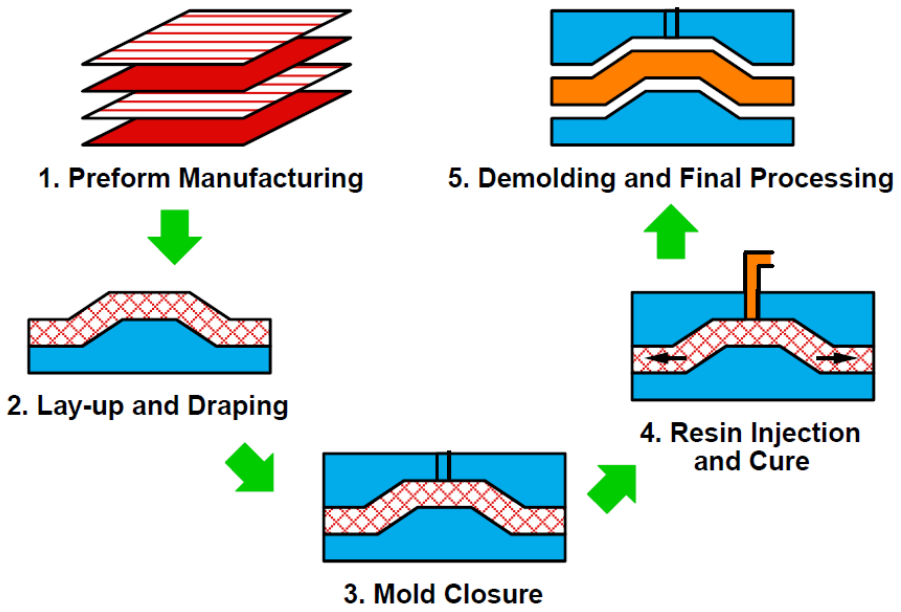

Figure 1.1: Process steps in RTM [1].

1.1.2 Vacuum Assisted Resin Transfer Molding (VARTM)

VARTM (see Figure 1.2) was derived from RTM. In contrast to RTM, there is one rigid mold part and the other part is a plastic film called vacuum bag. After the fabric preform is placed on the rigid mold part, a sealant tape (called tacky tape) is used to close the mold and plastic film. Instead of positive pressure injection as in RTM, vacuum pressure is generated in the mold by using a vacuum pump in VARTM. Vacuuming causes both compaction of fiber preform and driving of the thermoset resin into the fiber preform by creating a pressure differential between inlet reservoir and exit [3].

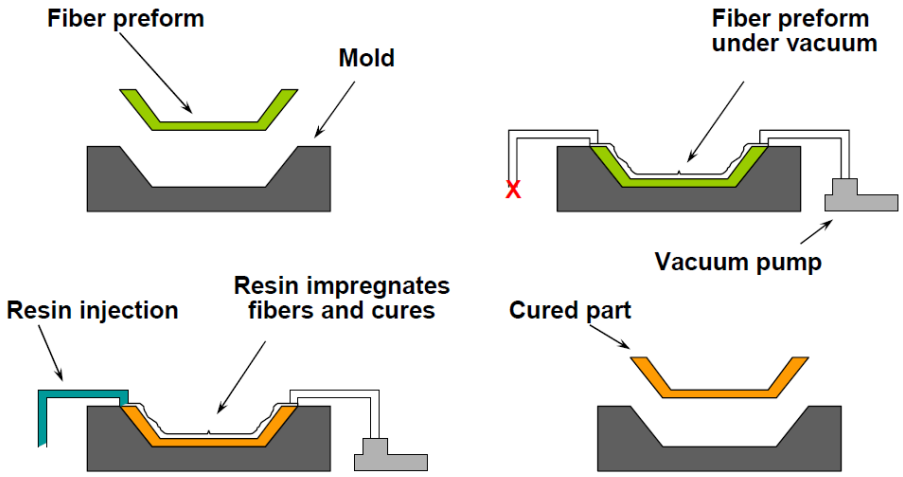

Figure 1.2: Process steps in VARTM [1].

1.1.3 Comparison between RTM and VARTM

VARTM has some advantages and disadvantages when compared to RTM. For instance, VARTM requires lower investment cost since it uses only one mold part and the top is covered with a vacuum bag which cuts down the mold tooling costs. In RTM, the cost of two matched mold parts increases as the size of the manufactured part increases, so VARTM is convenient for the production of complex and large-scale composite parts such as bridge sections, wind turbine blades and rail carriages; and thus mostly used in the automotive, defense, sport, and marine industries [1]. However, high surface roughness occurs because of the non-rigid upper mold (vacuum bag) in VARTM, whereas better surface finish is achieved in RTM. VARTM is carried out at low resin pressures (below atmospheric pressure, P_{atm}) because of the vacuum pump used which lowers the initial capital investment cost when compared to cost of high-pressure injection machines of RTM. Besides these advantages, VARTM has its disadvantages as it requires labor-intensive work such as vacuum bagging and lower fiber volume fraction and mechanical properties, higher dimensional variations and surface roughness compared to RTM.

1.2 Thickness variation in VARTM

Limited compaction pressure and thus low fiber volume fraction and mechanical properties is major drawback of VARTM. Besides this limitation, variation of part thickness (i.e., nonuniform thickness) is another important drawback of VARTM. Figure 1.3 shows fabric types used in which are random, woven, biaxial fabrics and core

material. As seen from the figure, they have different fiber structures which are non-uniform in random fabric but generally repeated (periodic) in woven and biaxial fabrics. Not only the fiber structure but nonrepeatable fabric cutting and placement into the mold cavity also causes variation in reinforcement material and thus final part thickness. The fabric thickness changes spatially and also with time during resin infusion in VARTM process. Because the upper non-rigid mold part (vacuum bag) is flexible and change in local resin pressure causes change in compaction pressure (see Eq. 1.1)

$$P_c = P_{atm} - P_r \tag{1.1}$$

As a result, thickness changes with time and spatially. Figure 1.4 illustrates pre-infusion stage in VARTM. After the infusion is started, as the resin pressure (P_r) increases with time at a location (which is the highest at the inlet), compaction pressure (P_c) decreases as seen in Figure 1.5. Part thickness (h) varies as a function of spatial coordinates and time, h(x,y,t).

In order to monitor the part thickness in VARTM process, there are some monitoring methods listed below section.

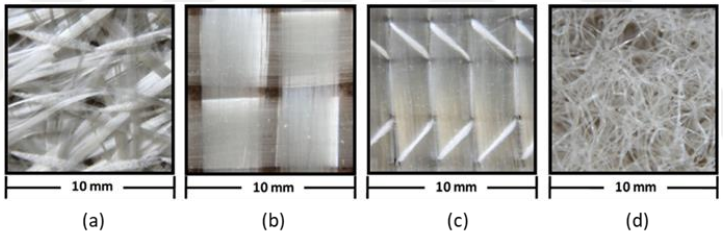

Figure 1.3: Fabric types (a) Random (stitched) fabric, (b) Woven (plain) fabric, (c) Biaxial (stitched) fabric, (d) Polypropylene Core [4].

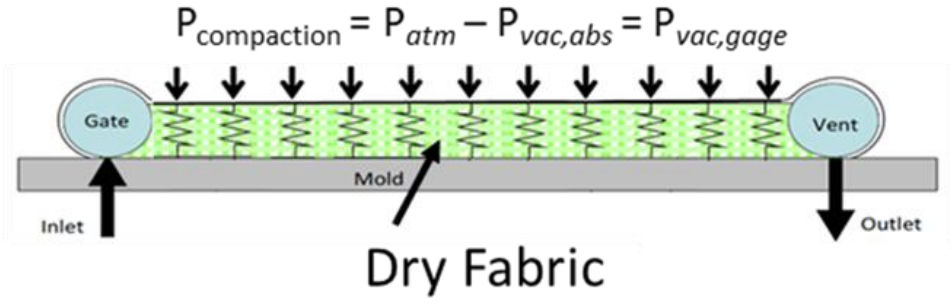

Figure 1.4: Schematic of VARTM process during initial vacuuming (when the preform is dry) [1].

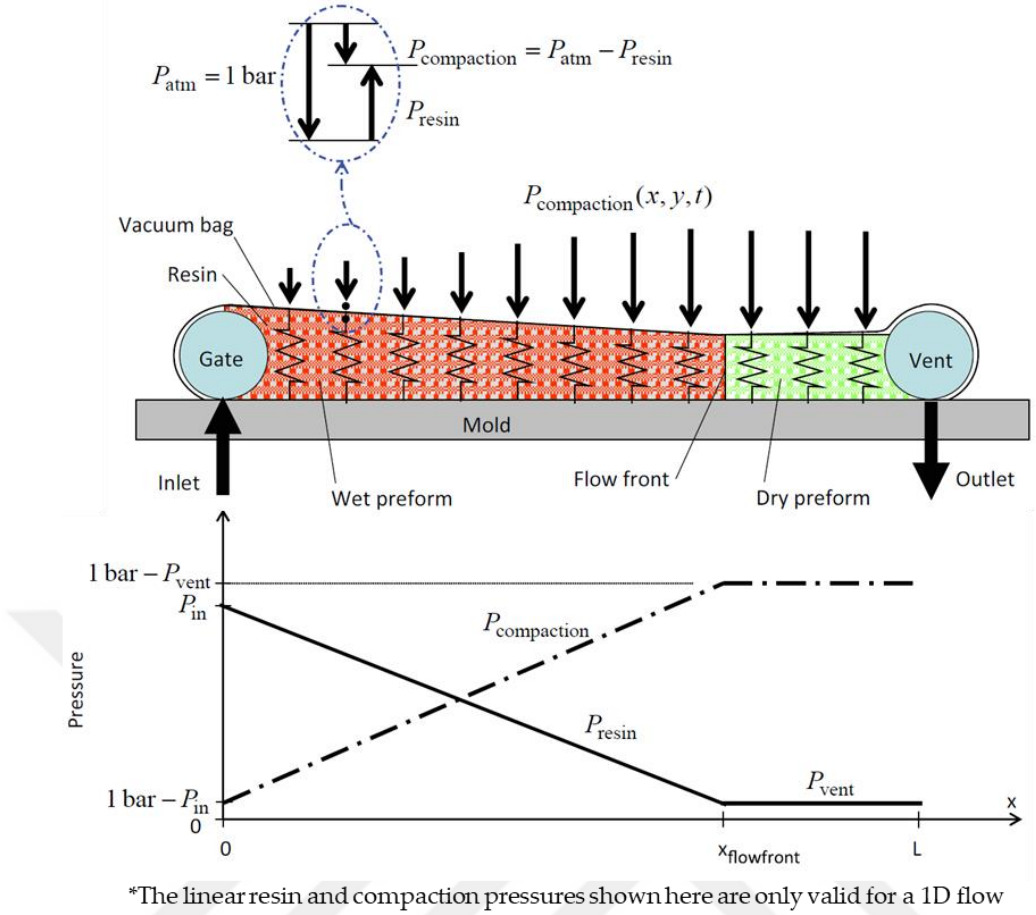

Figure 1.5: Schematic of VARTM process during flow propagation [1].

1.3 Thickness Monitoring Methods (Sensors)

Common sensor types to monitor part thickness are (i) dial gages, (ii) linear variable differential transducers (LVDT), (iii) laser displacement sensors, (iv) digital speckle photography (DSP), and (v) 3D scanners [5]. Dial gages and LVDTs contact with the part and may cause indentation at contact point and this may cause measurement inaccuracy. On the other hand, laser displacement sensors do not make mechanical contact with the preform, so they are capable of measuring thickness of the part by using a laser beam at a single location without disturbing the part. However, laser displacement sensors require a diffusive surface at the measurement point, so opaque tape or spray paint must be applied at measurement points on the vacuum bag [6]. Digital speckle photography (DSP) is an image processing technique, and it does not have a mechanical contact either. However, its resolution depends on the size of scanned area, thus it is not practical for large parts [6]. In this study, Structured Light Scanning (SLS) system is used for thickness monitoring and detailed information about the system is given in Section 1.3.1.

1.3.1 Structured Light Scanning (SLS)

3D scanning of objects has been developing rapidly in design, entertainment (such as model building for movies), animation and virtual reality applications, archaeology [7], industrial, architectural, civil surveying, urban topography, mining, reverse engineering, dentistry, and mechanical dimensional inspection [8]. Structured Light Scanning (SLS) is one of the predominant measurement technologies that can serve for the applications in these fields.

Structured Light Scanning allows full-field thickness monitoring of an object, so that this measurement is in a domain rather than a point. Also, it does not touch the object surface like dial gages and LVDTs. SLS system consists of a projector, a camera and a software program, DAVID [16]. SLS system can be seen in Figure 1.6. Projector illuminates the scanned domain (surface of an object) and projects stripe patterns as a series of structured light patterns, consisting of vertical black and white alternating stripes (see Figure 1.7). Initially (before the object is placed on the reference plane/mold), the camera captures these patterns and this reference data is stored. After the object is placed, the projector projects the stripe patterns onto the object. The surface of the object distorts these stripe patterns. The stripe patterns follow the curvature of the object and a new pattern is formed. This new pattern is captured by the camera. This scanner system (SLS) calculates the thickness distribution based on the distortion in the pattern [7]. Projection of the vertical black and white alternating stripes onto an object takes approximately 5 seconds in the setup used in this study. The series of patterns are projected as seen in Figure 1.8. Also, the scanner projects different patterns onto the scanned area for better accuracy.

In this study, SLS system was used in manual scanning format by sending a command from the MATLAB program asking the projector to send the patterns for 5 seconds and the camera to record the patterns simultaneously. In an automated alternative format, the full process can be scanned, a video is recorded, and each 5-second segment is analyzed sequentially.

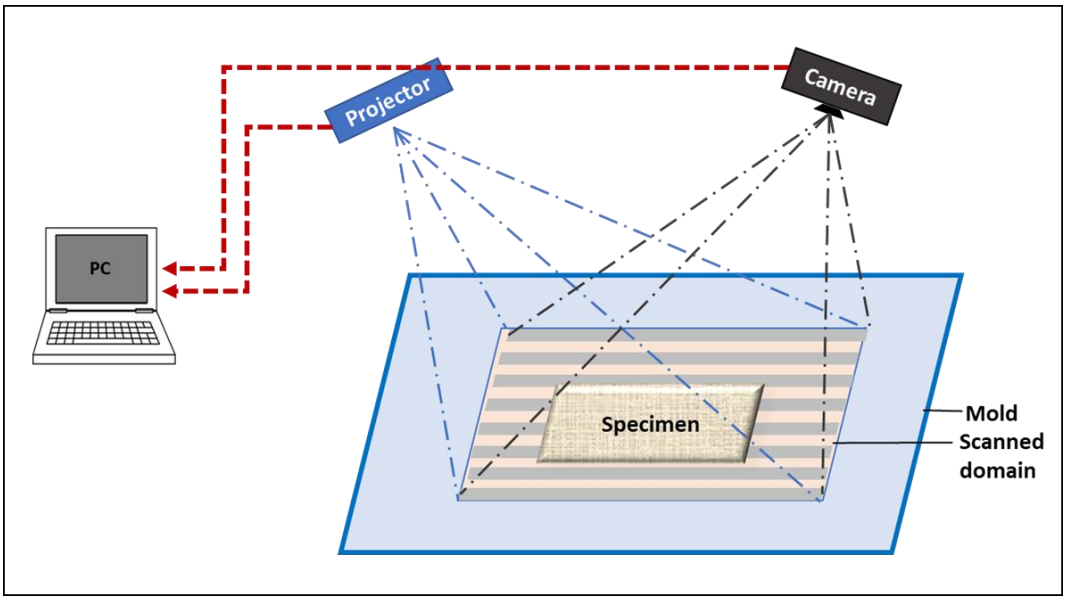

Figure 1.6: Structured Light Scanning (SLS) setup (adapted from Baris Caglar's PhD Thesis) [18].

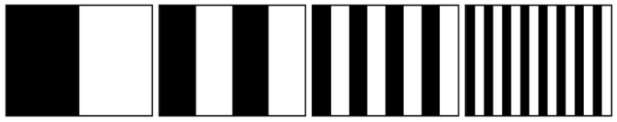

Figure 1.7: Vertical black and white stripe patterns used in SLS.

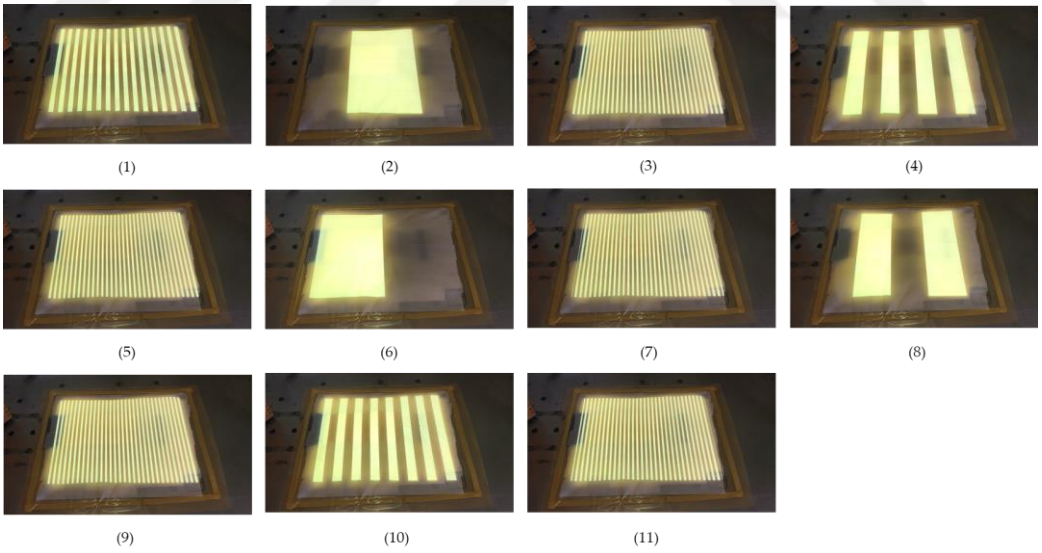

Figure 1.8: Stripe patterns projected onto an object in SLS system. Numbers show the pattern sequence during a single scanning.

Calibration of the SLS system

Calibration of the system is performed before the scanning step and it is done with the help of a V-shaped calibration panel (see Figure 1.9). The V-shaped panel has an orthogonal pair of calibration plates which contains six rings (need to be visible to the

camera) and several other points (to extend out of field) which are used for calibration purpose [19].

Figure 1.9: V-shaped panel for calibration of the SLS system.

Technical specifications of SLS setup

Casio XJ–A140 projector and Canon EOS 550D camera are used. Their specifications are given in Table 1.1. After zoom and focus of projector are adjusted, camera connection is checked, and DAVID software is started. In DAVID, screen ID and camera are chosen, and calibration step is accomplished using calibration V-shaped panel. Then, scanning process is started (see Appendix A for software interface).

Table 1.1: Technical specifications of camera and projector.

Parameter	Specifications
Camera	Canon EOS 550D
Camera Resolution	5184 x 3456 pixels (18.0 megapixels)
Camera Lens Focal Length	50 mm
Camera Lens Aperture	Max aperture 1:2.5
Projector	Casio data projector XJ – A140
Projector Resolution	1024 x 768 pixels

Accuracy of the SLS system

A Johnson gauge block with in-plane dimensions of 100 mm x 20 mm, and a thickness of 6±0.01 mm is used to measure the accuracy of the SLS system (see Figure 1.10).

The gauge is scanned three times to investigate three alternative surfaces: i) white tape on the gauge, ii) paper tape on the gauge, and iii) original metal surface. Johnson gauge is located at the center of the scanned area. Average of each scan on 10x80 mm^2 area for 3 different surfaces are tabulated and shown in Table 1.2. Standard deviation of the measurements corresponding to the metal surface of the test piece is higher than when the specimen is covered with either white tape or paper tape. This is expected to be due to reflected light from the metal surface. Moreover, it is scanned from slightly different positions to see the measurement accuracy at different distances from camera. White-tape-coated test piece is scanned three times at 6 different locations (see Figure 1.11) like before and seen that the average thickness is under-evaluated while moving away from camera as tabulated in Table 1.3. Scanning the white-tape-coated test piece is repeated twenty times for the same x position every 15-second intervals for 300 seconds to check the repeated measurements' reliability. That means the 10x80 mm^2 area (800 nodes) is scanned 20 times. The average thickness measurement changes between 6.00 mm and 6.04 mm. The average of 20 scans (i.e., 20 scans x 800 nodes = 16000 data) is 6.02 mm with a standard deviation of 0.02 mm; and the maximum and minimum values are 6.08 mm and 5.87 mm, respectively. The SLS software (DAVID) is adjusted so that the mesh nodes are positioned on the specimen surface. Average thickness of the white-tape-coated object is measured as 6.01 mm with a standard deviation of 0.03 mm at the center.

In this study, all the SLS thickness measurements were conducted by covering the vacuum bag with a paper tape except this part. Also, in all experiments in Chapter 2 (*Compaction Characterization Experiments*), the test piece (see Figure 1.10) is placed inside the vacuum bag to check the scanning system accuracy. Total thickness of vacuum bag and paper tape (0.20 mm) is included in all values that will be presented in this study.

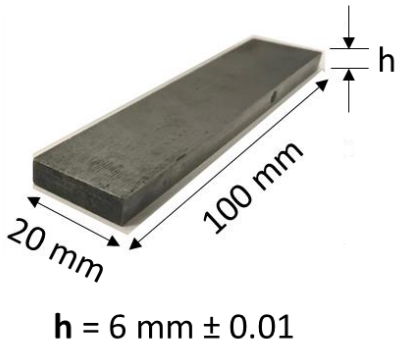

h = 6 mm ± 0.01

Figure 1.10: Johnson gauge block to determine the accuracy of the SLS system used.

Table 1.2: Comparison of thickness data (in mm) of different coated test piece.

	White tape	Paper tape	Metal surface
Mean	6.01	5.97	5.96
Standard deviation	0.03	0.02	0.05
Maximum	6.07	6.02	6.19
Minimum	5.92	5.90	5.84

Table 1.3: Thickness data (in mm) of test piece (white-tape-coated) at different locations (std stands for standard deviation).

	Position 1	Position 2	Position 3	Position 4	Position 5	Position 6
Mean	5.95	5.99	6.01	6.04	6.06	6.05
Std	0.03	0.02	0.03	0.05	0.01	0.03
Maximum	6.02	6.04	6.07	6.09	6.09	6.15
Minimum	5.88	5.92	5.92	5.69	6.01	5.98

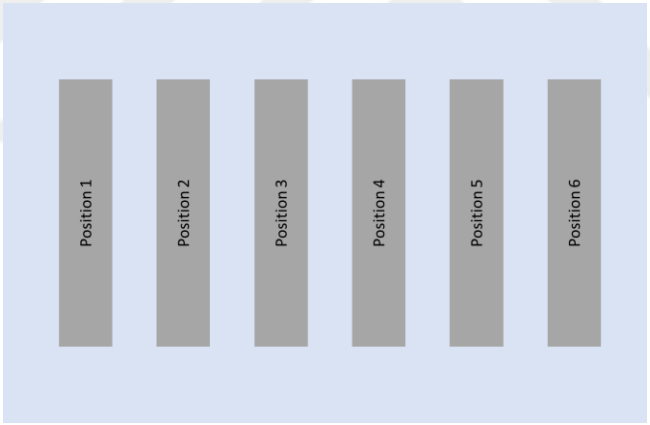

Figure 1.11: Scanning positions referred in Table 1.3 as seen from the top of the mold.

1.4 Materials Used

1.4.1 Fabrics

Conventional reinforcement fabrics are made of glass, carbon or aramid fibers; fiber bundles are usually weaved or unidirectional, depending on the needs. Glass fibers have lower cost and dominate the market, but carbon and aramid fibers have superior mechanical properties like higher stiffness and strength [1]. Instead of using fabrics made of these fibers, in this study a dummy material will be used: Metyx Metycore PP

(Polypropylene) due to its preparation (cutting/placement) convenience. This core material was used as a test fabric in this study because of the following reasons: (i) it is easy to cut and handle and therefore allows almost repeatable fabrication process and experiments, and (ii) it is healthier because core material does not have fibers which may cause itching on hands. As explained in the introduction section, inherent deformations and irregularities in fabric rolls can cause variations in tow structure. Thus, the use of core material instead of actual fabric material will eliminate the significant variation in the experimental results. Also, the experiments of this thesis are designed to observe and minimize the thickness variation in VARTM process by using dummy material instead of manufacturing actual composite parts. The core material is purchased from Metyx and has a superficial density of ρ_{sup} = 0.150 kg/m^2 per layer.

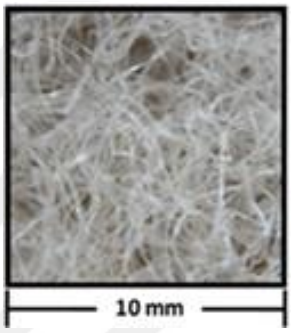

Figure 1.12: Metyx Metycore Polypropylene core material [4]

1.4.2 Test Fluid

In LCM processes, usually thermoset resins such as polyester and epoxy are used due to their lower viscosity compared to thermoplastic polymers. In this study, silicon oil is used as a test fluid instead of an actual thermoset resin. Because, this study aims to model and observe how a porous reinforcement is compacted under loading and liquid resin flows through the reinforcement; and it does not aim to manufacture a finished product. Silicon oil is used as the test fluid for the following reasons: (i) after each experiment, cleaning of silicon oil is easier, (ii) being chemical friendly, (iii) does not have odor making it healthier, (iv) easy to handle, and (v) does not stick to or damage pressure sensors mounted on the mold plates. Viscosity of the silicon oil used in this study is around 0.10 Pa.s at room temperature which is similar (in the order of magnitude) to the viscosity of a typical polyester resin.

1.5 Literature on Process Control

As mentioned earlier in Section 1.2, when resin propagates through a porous medium in VARTM, compaction pressure on the medium changes as the resin pressure changes locally. Because of that, part thickness (h) varies with time and with spatial coordinates, $h(x,y,t)$. There are some process control methods to minimize the variation and to achieve an almost uniform part thickness.

Resin bleeding is a commonly used method to decrease the thickness variation in the part being manufactured. In resin bleeding, after the mold is completely filled with resin, the injection gate(s) are closed, and vacuuming is continued through the ventilation port(s). This approach helps to drain out excessive resin from the system. In addition, part thickness decreases and fiber volume fraction increases, and thus final mechanical properties increase as the excessive resin exits the mold. Also, overall thickness variation decreases because both resin and compaction pressures start settling when the inlet is closed; however, it may take minutes to hours to reach almost uniform pressure distribution. On the other hand, resin bleeding causes higher resin wastage as most of the resin bleeds through the exit port, but this could be prevented with controlled experiments [9][10].

Another method to decrease the thickness variation in the part is debulking. Debulking is applied before the resin infusion by repeated compression – relaxation cycles on a dry fabric preform. These cycles help to increase compaction of the fiber preform and thus increase the fiber volume fraction while decreasing the overall thickness variation [6][11].

1.6 Compaction Characterization Models

Compaction characterization experiments and models have been studied by many researchers. Purpose of the compaction characterization is to monitor and model the thickness change in the fabric preform as compaction pressure changes. There are two types of compaction characterization models. They could be either elastic or viscoelastic compaction models. The most common fabric compaction characterization model is elastic model because of its simplicity. It is a static relationship between compaction pressure and part thickness (and thus fiber volume fraction) and viscous behavior is ignored. When compaction pressure changes to a new and constant value, thickness changes instantaneously, that means the response occurs immediately, so does not take

time. Power law method (Eq. 1.2) is the most common approach in elastic compaction characterization model which relates compaction pressure, P_c and fiber volume fraction, V_f.

$$V_f = CP_c^D \tag{1.2}$$

where C and D are constants and determined from the experimental data by curve fitting.

Contrast to elastic models which are not time dependent, viscoelastic models are time dependent. In actual VARTM process, part thickness varies with time even when local pressure is almost constant, therefore the actual fabric compaction behavior is viscoelastic. Maxwell, Kelvin-Voigt, Zener, Burgers and Generalized Maxwell are common viscoelastic models [12]. In Yenilmez's study [4], viscoelastic behavior becomes substantial at low compaction pressures under 20 kPa, and thickness does not reach a steady value even after minutes to hours.

Chapter 2:
COMPACTION CHARACTERIZATION EXPERIMENTS

2.1 Introduction

One of the major drawbacks of VARTM is thickness variation in the finished composite part. This thickness variation can occur because of (i) inherent variations in the material due to non-uniform and irregular fabric structure and (ii) variation in resin pressure (which is maximum near the inlet and minimum near the exit) which causes variation in compaction pressure. Thickness varies as a function of spatial coordinates and time, h(x,y,t) because of the non-rigid vacuum bag. Detailed information is given in *Thickness Variation in VARTM* section in Chapter 1.

Compaction characterization is conducted to relate a material's compaction behavior, that means how its thickness and thus fiber volume fraction, V_f changes as the compaction pressure, P_c acting on it changes. This is more important in VARTM than in RTM. In RTM, the mold cavity can be assumed constant when the mold parts are closed. There may be small or insignificant part deflections (and thus part thickening) due to resin pressure during resin injection (mold filling). VARTM is more vulnerable to resin pressure due to the flexible vacuum bag used as the upper mold part. In industry, the general solution to the thickening of the part due to resin pressure is to apply resin bleeding after complete mold filling (by closing the inlets and keeping the exits open). This allows settling of the resin pressure inside the mold and thus settling the part thickness. However, it is difficult to estimate how much time it takes for this homogenization; and many researches showed that it is much longer than minutes. Besides, applying this post filling procedure for an excessive time duration may cause resin starving regions and thus decrease in the final mechanical properties. So, one needs to understand the scientific knowledge underneath the compaction behavior of fabric preforms, and preferably couple it with the resin flow in the process modeling.

2.2 Compaction Characterization Experimental Setup

Figure 2.1 shows the compaction characterization experimental setup with thickness monitoring system used in this study. The setup includes a vacuum pump, electronic vacuum regulator, SLS system, a mold and fabric preform. The resin trap (see Figure 2.1) is not used in compaction characterization experiments but will be used later in mold

filling experiments. The vacuum pump is used to compact the fiber preform. SMC ITV2090 electronic vacuum regulator with a regulating pressure range of 1.3 – 80 kPa is controlled via a computer to adjust the compaction pressure (see Appendix B for vacuum regulator specifications). Refer to Yalcinkaya's study [13] for technical details of SLS system used for full-field thickness monitoring. Detailed information about fabric and preparation steps is given in the upcoming sections.

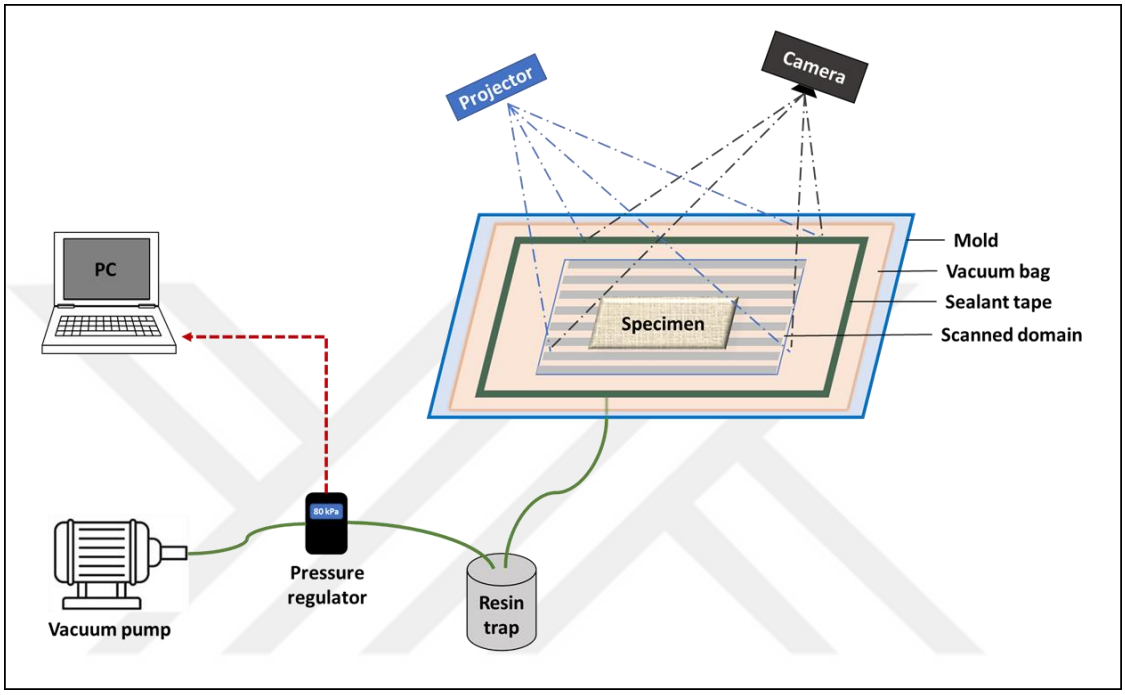

(a)

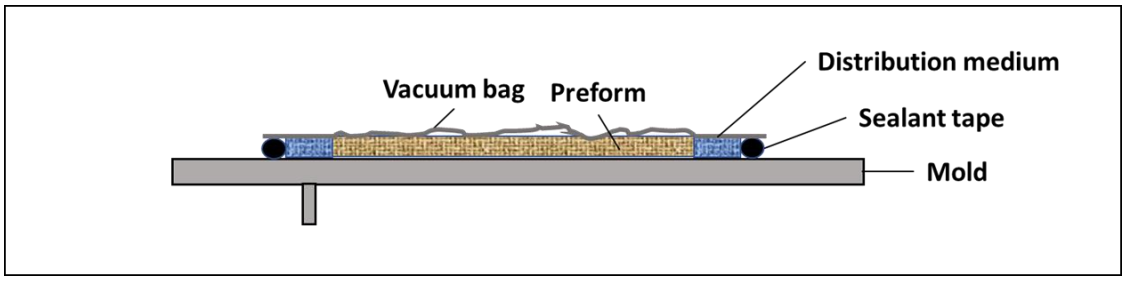

(b)

Figure 2.1: (a) Compaction characterization experimental setup with thickness monitoring system, (b) side view of the mold (adapted from Baris Caglar's PhD Thesis) [18].

2.2.1 Fabric

In Chapter 1, information about the dummy fabric is given. Here in this section, its dimensions and preparation steps will be detailed.

In compaction characterization experiments, dimensions of the specimens are 200 mm (in flow direction that will be conducted later) and 100 mm in width. Figure 2.2 shows a Polypropylene (PP) core material used in this study. It has a superficial density, ρ_{sup} of 0.150 kg/m^2 per layer. Fabric specimens are made of 1, 2, 3 or 4 layers (see Figure 2.3).

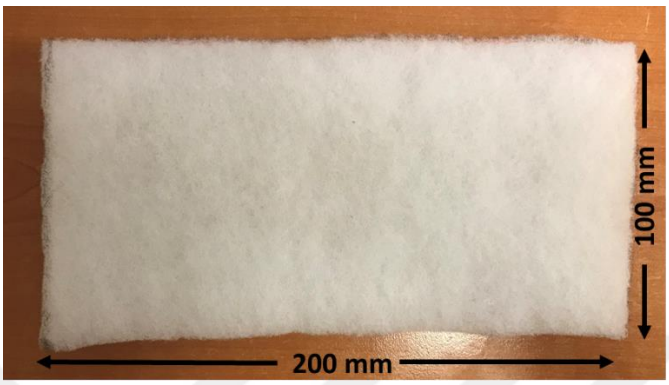

Figure 2.2: Dimensions of core material used in compaction characterization experiments.

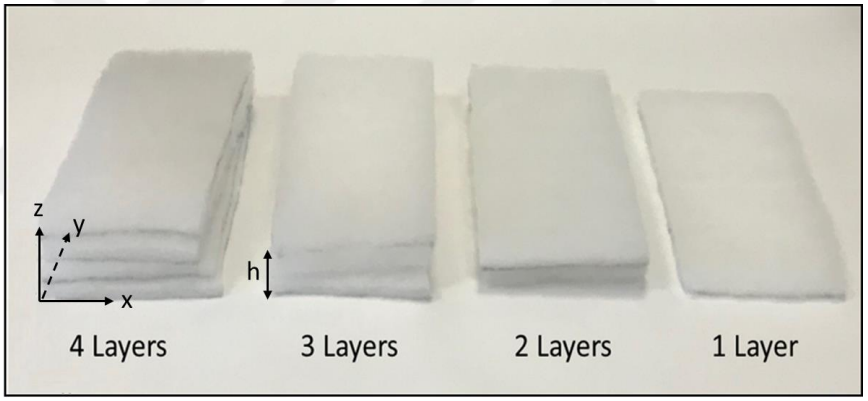

Figure 2.3: Specimens made of 1, 2, 3 and 4 layers of core material.

Preparation steps

Preparation steps just before a compaction characterization experiment is illustrated in Figure 2.4 and described below.

(a) Top view of the flat mold (circles are pressure sensors placed at the bottom plate of the mold; they will be used in mold-filling experiments),

(b) White tape is coated (pressure sensors are useless for compaction characterization experiments; they are covered with white tape. This flat surface is used as a reference plane),

(c) Sealant tape is used to close the mold and vacuum bag,

(d) Flow mesh is placed near the inlet to accomplish 1D resin flow,

(e) Fabric preform (which is core material in this thesis) is placed,

(f) Test piece is placed to check the accuracy of the thickness measurements,

(g) Vacuum bag is placed to envelope the tool,

(h) Tape coating is applied on the bag in order to decrease reflection,

(i) Illumination by the projector on the scanned domain.

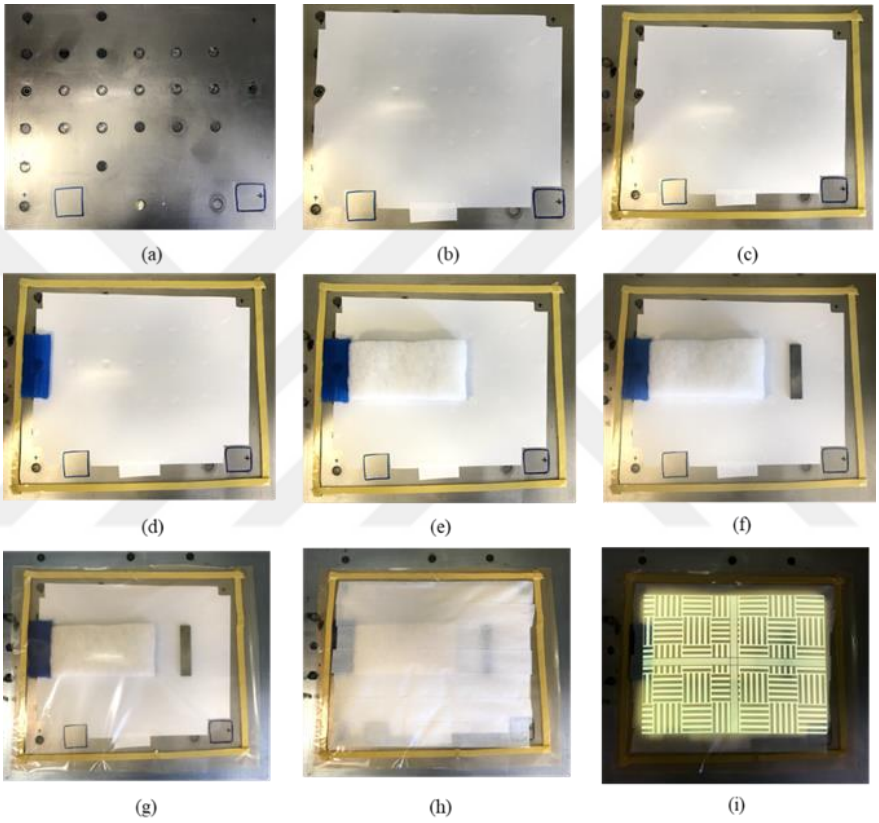

Figure 2.4: Preparation steps of the setup for compaction characterization experiments.

2.3 Compaction Characterization Experiments

Compaction characterization experiments are conducted for 1, 2, 3 and 4 layers of core material at an increasing trend of 2, 5, 10, 20, 40, 60, and 80 kPa pressure levels, and also backward (at a decreasing trend of 80, 60, 40, 20, 10, 5 and 2 kPa pressure levels). These experiments are conducted on dry core material specimens. Scanning is repeated twice by starting at t = 30 seconds and 60 seconds of each pressure level. Each scanning takes place approximately 5 seconds. Figure 2.5 displays how an experiment is conducted

for loading stage. Red line represents the scanning by SLS which takes place in 5 seconds. For example, pressure is set to 2 kPa, scanning is performed twice in 30 – 35 and 60 – 65 seconds. Approximately 10 seconds is reserved for saving the data to a file and changing the pressure level to the next value. Each compaction characterization experiment is performed five times for 1, 2, 3 and 4 layers of core material specimens.

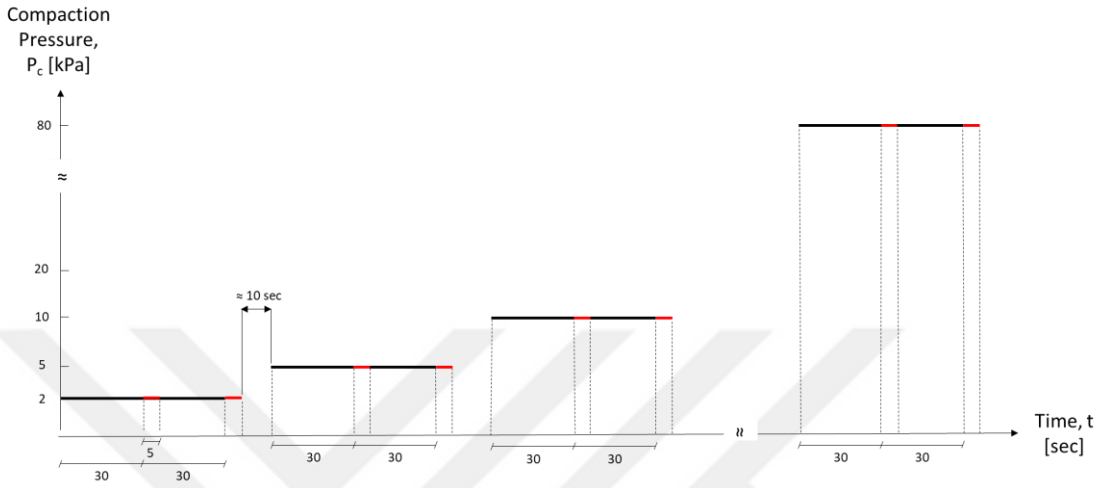

Figure 2.5: P_c versus t graph of a compaction characterization experiment.

In these compaction characterization experiments, a flow mesh, specimen (core material) and a test piece are used as seen in Figure 2.6.

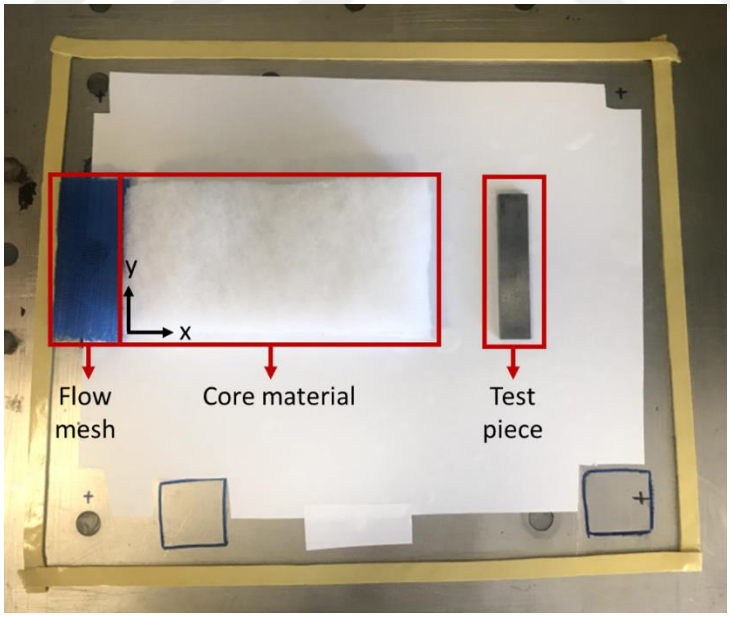

Figure 2.6: Materials (flow mesh, core material, test piece) placement on the mold.

1-, 2-, 3- and 4-layer core materials placed on mold and then compaction pressure applied on it. It starts from 2 kPa increasing till 80 kPa, this part is called compaction. In different terminology, it is called as loading. Then, decompaction is achieved, meaning

that the pressure value is decreased from 80 kPa to 2 kPa. This part is called decompaction or unloading.

In the Figure 2.7, the red star represents the average thickness of the selected area and blue bar represents plus minus standard deviation, black star above and below standard deviation shows maximum and minimum values, respectively. In this part of the thesis, 5 experiments are performed for 1, 2, 3 and 4 number of layers at 30 and 60 seconds. There is some accumulation on the edges because of vacuum bag coverage, whole specimen area is not chosen in the calculation of the average thickness value of the core material. Instead of whole specimen area 200x100 mm^2 (41x21 nodes), an area of 45x45 mm^2 is chosen which is equivalent to 10x10 nodes. As a result, average thickness in the Figure 2.7 is the average thickness of 10x10 nodes (45x45 mm^2) within the scanned area for all cases (a stack of 1, 2, 3, or 4 layers of core material) (see Appendix C for the effect of chosen area).

Fiber volume fraction, V_f is calculated using the Eq. 2.1. *n* is the number of layers, *h* is the thickness of the specimen, ρ_{sup} and ρ_f are superficial density of a single layer core material and polypropylene (bulk) density, respectively. *h* is thickness of the 10x10 nodes of every compaction characterization experiments.

$$V_f = \frac{n\,\rho_{sup}}{\rho_f\,h} \tag{2.1}$$

Figure 2.8 shows the fiber volume fraction, V_f versus compaction pressure, P_c (average thickness, standard deviation, maximum and minimum of 5 experiments for every layer as seen in the figure). Figure 2.9 and 2.10 represent the fiber volume fraction graph and model fit for loading and unloading stages. Exponential curve fit, $V_f = C{P_c}^D$ is used to find C and D using the least square method. Error bars shown with blue is the standard deviation in five repeated experiments for each layer. Fiber volume fraction, V_f is unitless and P_c is in kPa in the compaction model.

As the compaction pressure increases, thickness decreases. As seen from mean values on the graph, the change in thickness from 60 to 80 kPa is much smaller than the change from 2 to 5 kPa. There is no significant change in fiber volume fraction when the 30-s and 60-s measurements are compared indicating that the viscous behavior is not significant unless a longer time (15 minutes) is analyzed. The fiber volume fraction of the test material is approximately 22-23% under 80 kPa compaction pressure as seen in Figure 2.8. Thickness increases as number of layers increases. However, number of layers

and thickness are theoretically proportional as seen in Eq. 2.1. Because of that, fiber volume fraction is almost same for all cases (1-, 2-, 3- and 4-layer cases).

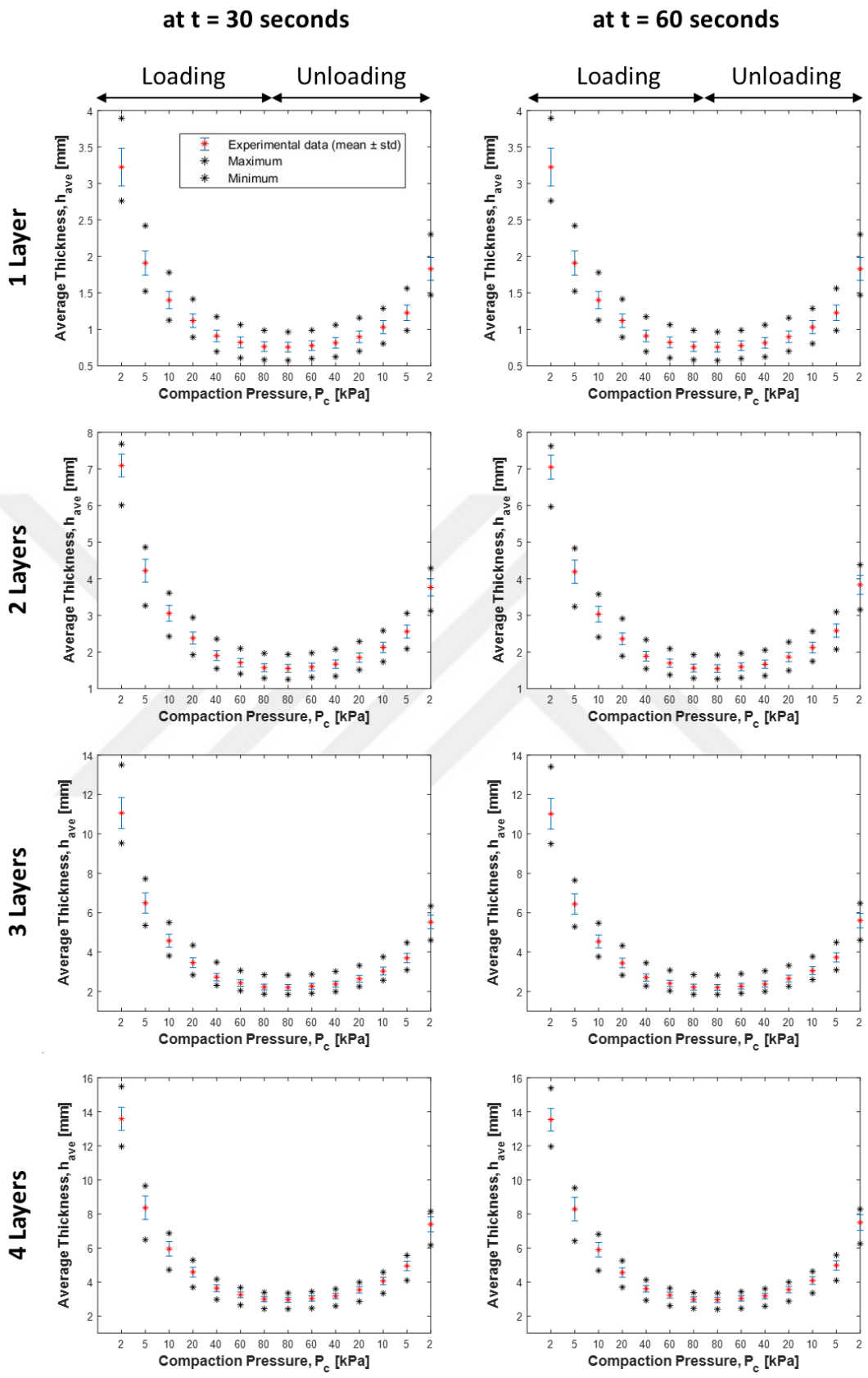

Figure 2.7: Average thickness, h_{ave} vs compaction pressure, P_c during compaction characterization of 1, 2, 3 and 4 layers specimens at 30 and 60 seconds for 10x10 nodes.

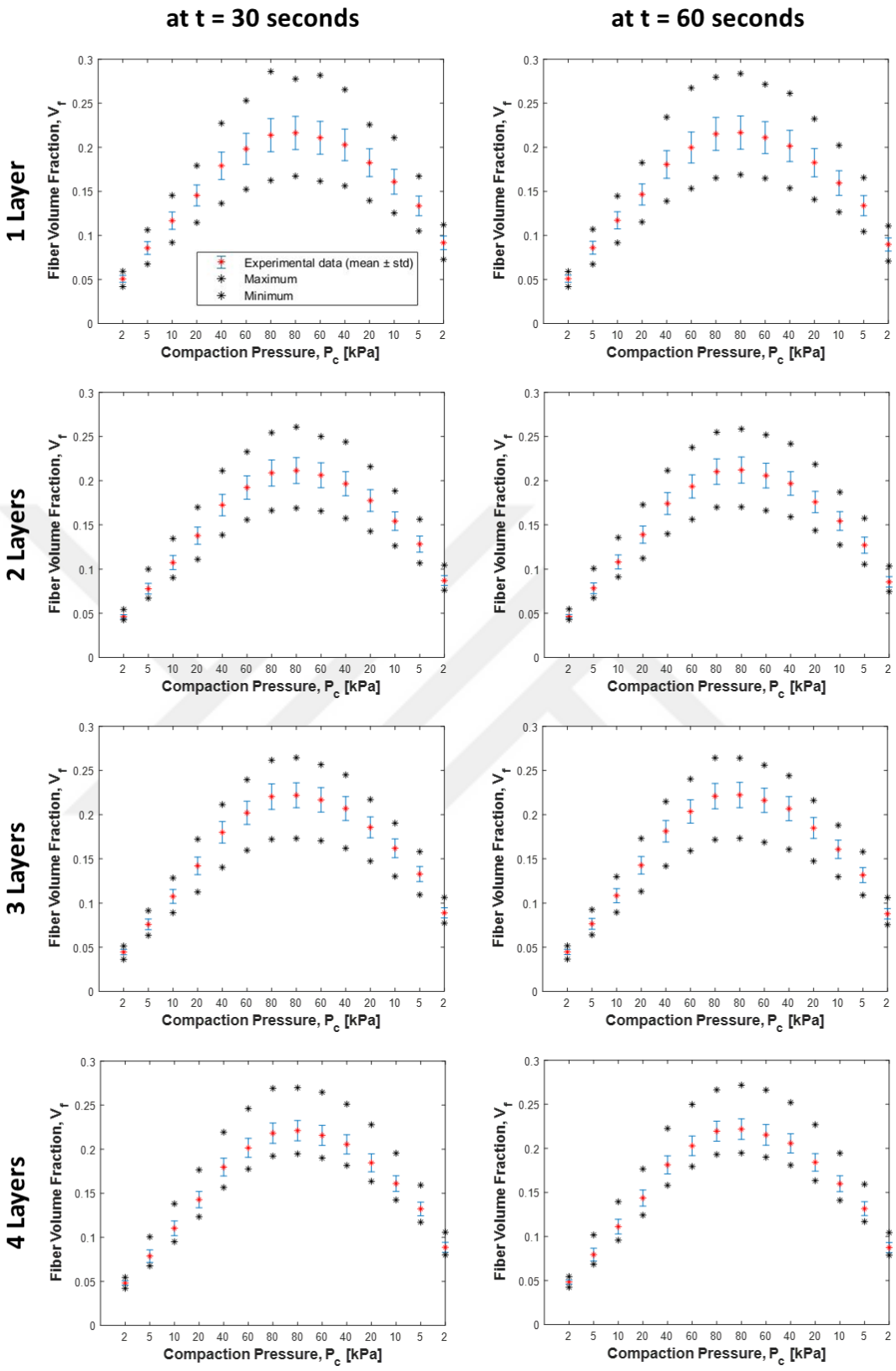

Figure 2.8: Fiber volume fraction, V_f vs compaction pressure, P_c during compaction characterization of 1, 2, 3 and 4 layers specimens at 30 and 60 seconds for 10x10 nodes.

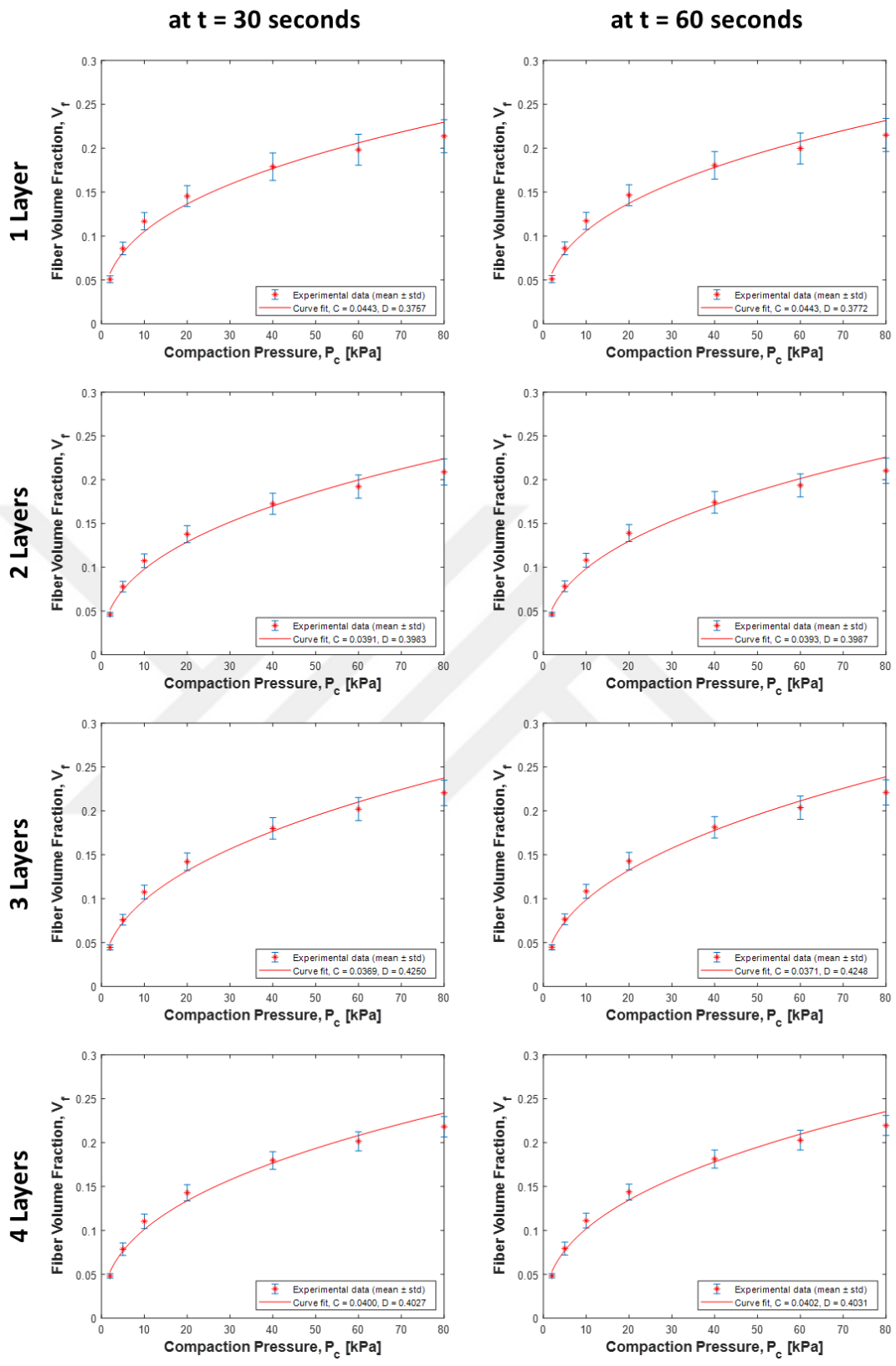

Figure 2.9: Fiber volume fraction, V_f vs compaction pressure, P_c during compaction characterization of 1, 2, 3 and 4 layers specimens at 30 and 60 seconds for 10x10 nodes – Compaction characterization experiments and curve fits of the experimental data (Loading).

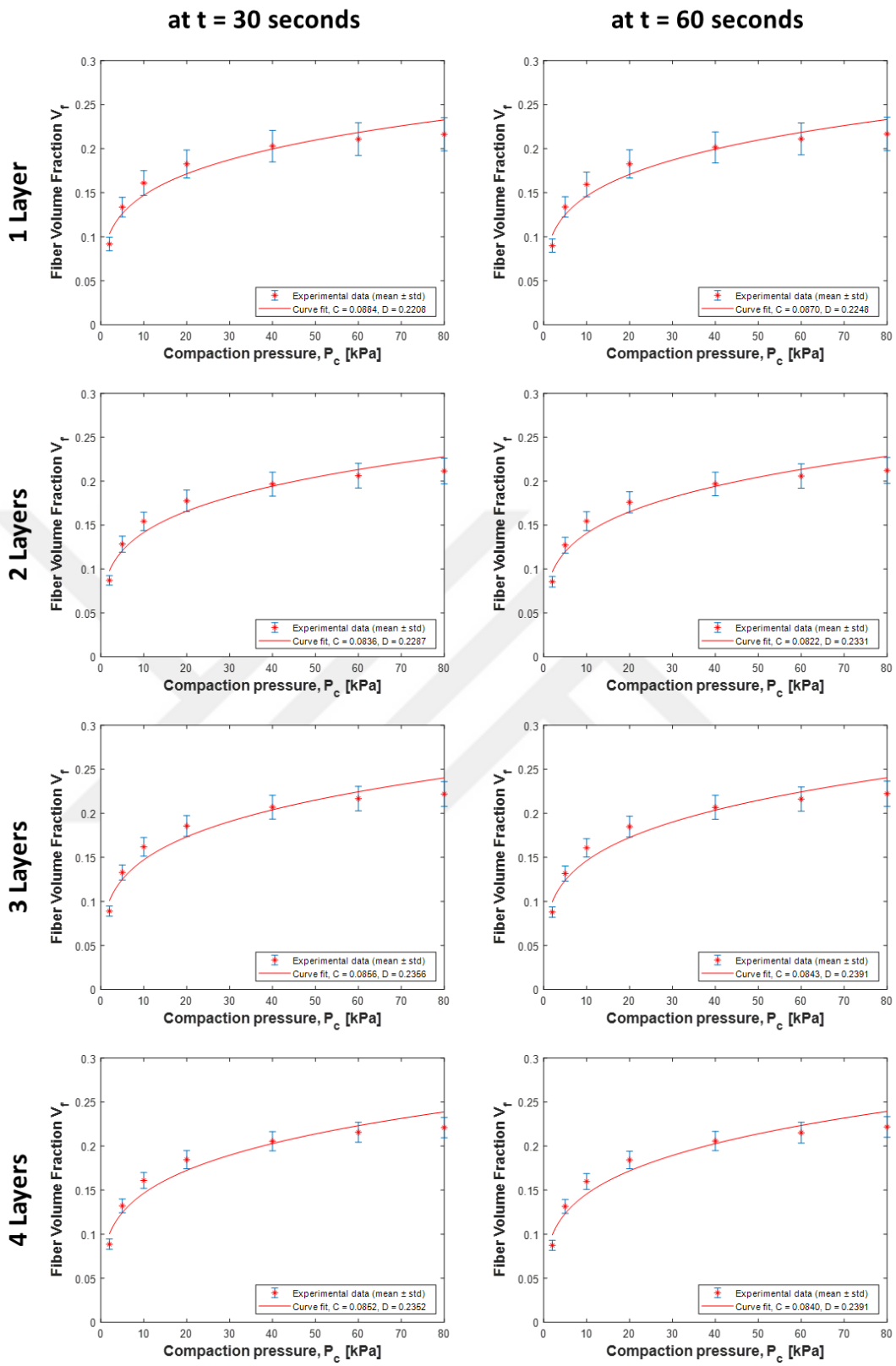

Figure 2.10: Fiber volume fraction, V_f vs compaction pressure, P_c during compaction characterization of 1, 2, 3 and 4 layers specimens at 30 and 60 seconds for 10x10 nodes - Compaction characterization experiments and curve fits of the experimental data (Unloading).

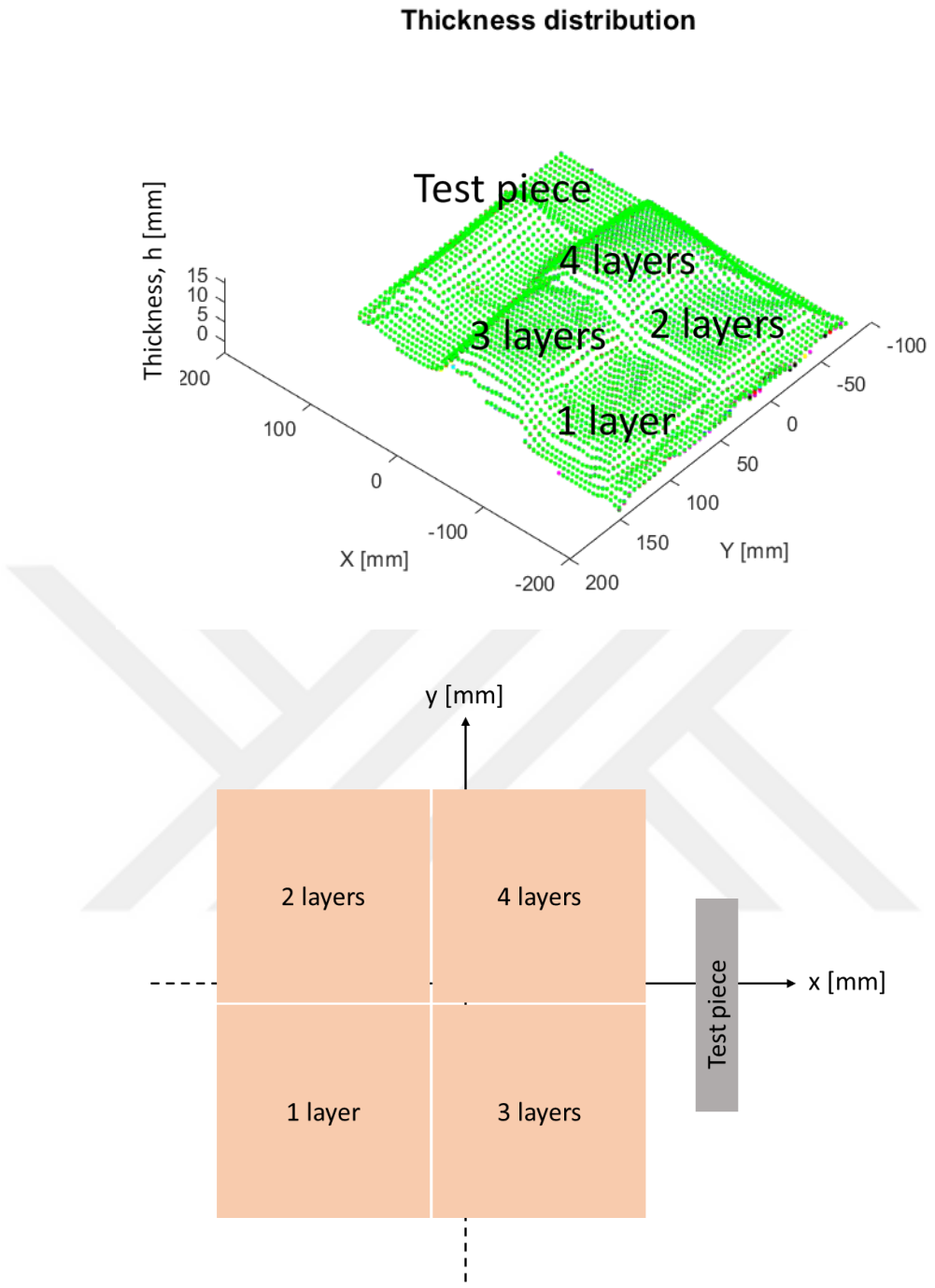

Figure 2.11: Thickness distribution graph of 1, 2, 3, 4 layers specimens and test piece for viscoelastic experiment.

In this part of the experiments, core material is cut in the dimensions of 100x100 mm^2 for 1, 2, 3 and 4 layers separately. Specimens and the test piece are placed on the mold as shown in Figure 2.11. Compaction pressure is set to 2, 5, 10, 20, 40, 60, 80 kPa and then backwards. For example, when compaction pressure is set to 2 kPa and 60 seconds is waited for settling of the core material thickness, and then scanning is done at every 15 seconds until the 900 seconds (i.e., at 60, 75, 90, 105, …, 875 and 900 s). This

step is conducted for both loading and unloading stages at given compaction pressure values. In Figure 2.12, red stars represent the average thickness, h_{ave} of 5x5 nodes for every compaction pressure value (2, 5, 10, 20, 40, 60, 80 kPa and backward) during 900 seconds for every layer of specimens, blue bars represent standard deviations. As seen from Figure 2.12, thickness at 2 kPa of unloading is very different than the thickness at 2 kPa of loading which means that the full thickness recovery has not been achieved. This is due to the fact that this material behaves as viscoelastic, meaning that if unloading at 2 kPa is continued for hours or days, thickness value may come back to the original thickness (full recovery), but this takes too much time. Under constant compaction pressure, thickness ratios of 1-, 2-, 3- and 4- layer specimens are approximately, but not exactly equal to 1, 2, 3 and 4, respectively. The deviation from the theoretically expected ratios is due to different levels of compaction, and thus nonuniform compaction of material in the thickness direction. It is a known fact that strain in loose and porous materials is not uniform. However here in this study, the deviation is rather insignificant. This is because the test material is a core material which is much more uniform compared to fiber fabrics in which nesting fiber bundles may cause more significant deviations from the aforementioned thickness ratios.

Also, dh/dP_c (i.e., the rate of change in thickness with compaction pressure) is higher at lower compaction pressures than higher compaction pressures. In addition, change in thickness during unloading stage is lower than the initial loading stage.

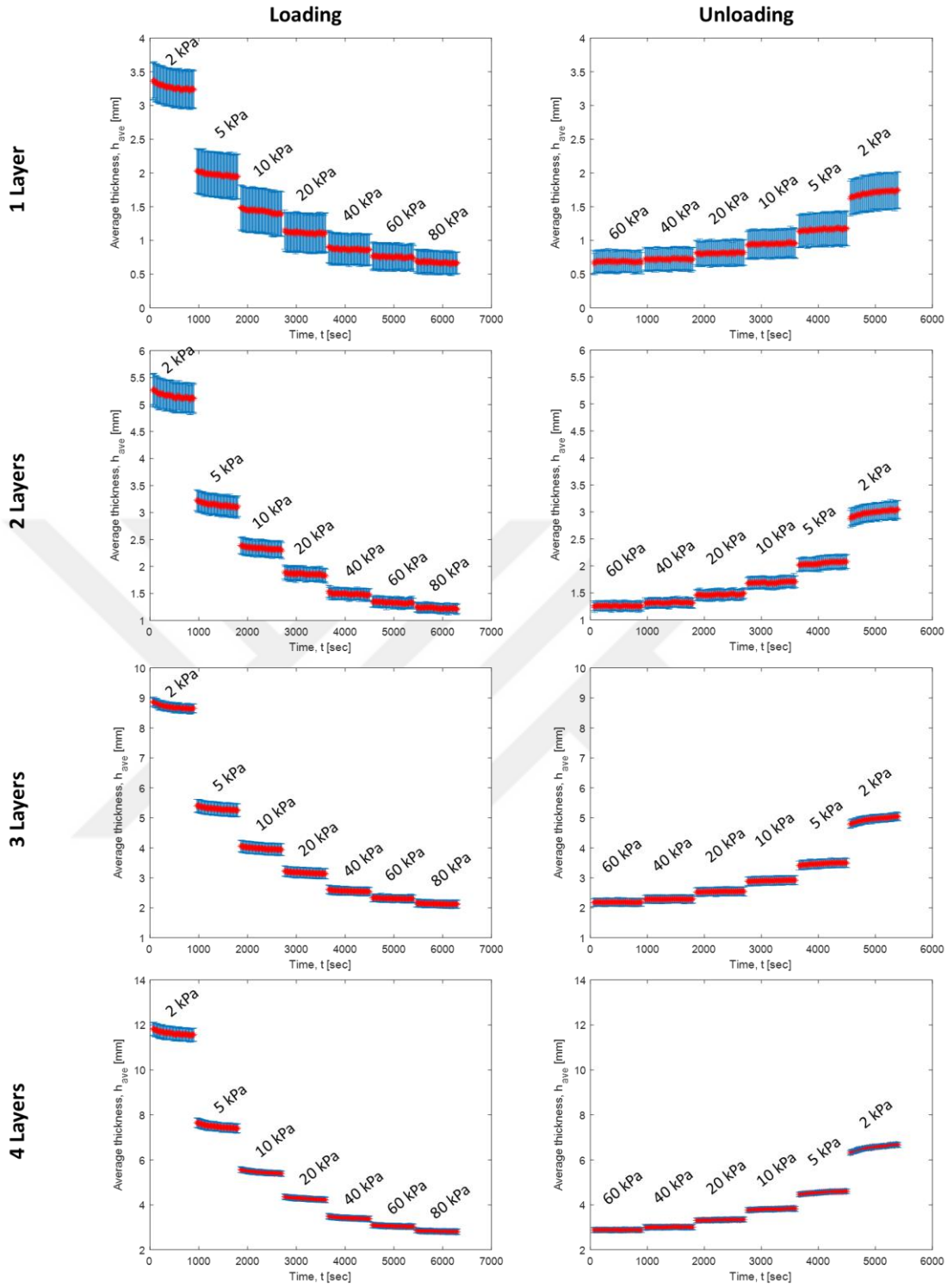

Figure 2.12: Average thickness, h_{ave} versus time, t during compaction characterization for 1, 2, 3 and 4 layer specimens documented for loading and unloading.

Chapter 3:
MOLD FILLING EXPERIMENTS

3.1 Mold-Filling Experimental Setup and Materials

Figure 3.1 shows Vacuum Assisted Resin Transfer Molding (VARTM) experimental setup which is the same as the compaction characterization experimental setup, except that a resin container is added here for infusion. In addition, pressure sensors are embedded to the flat mold to monitor the resin pressure during mold filling. Detailed information about sensors are given below.

Sensors: The system consists of 10 piezoelectric pressure sensors. Sensors (S_{01}, S_{02}, S_{03}, S_{04}, S_{05}, S_{06}, S_{07}, S_{08}, S_{09}, S_{10}) are shown in Figure 3.2. These sensors are used to monitor pressure distribution at x = 60, 120, 180, 240, 300 mm (0 position is the resin inlet center). The pressure measurement range is from 0 to 100 kPa with an accuracy of ± 0.3 kPa. Each sensor is placed 60 mm apart from each other in vertical and horizontal axes.

Resin: Silicon oil is used as test fluid with a viscosity of around 0.10 Pa.s at room temperature.

Material: Core material is used as in compaction characterization experiments. 1D and 2D VARTM Experiments is conducted on 2 layers of core material.

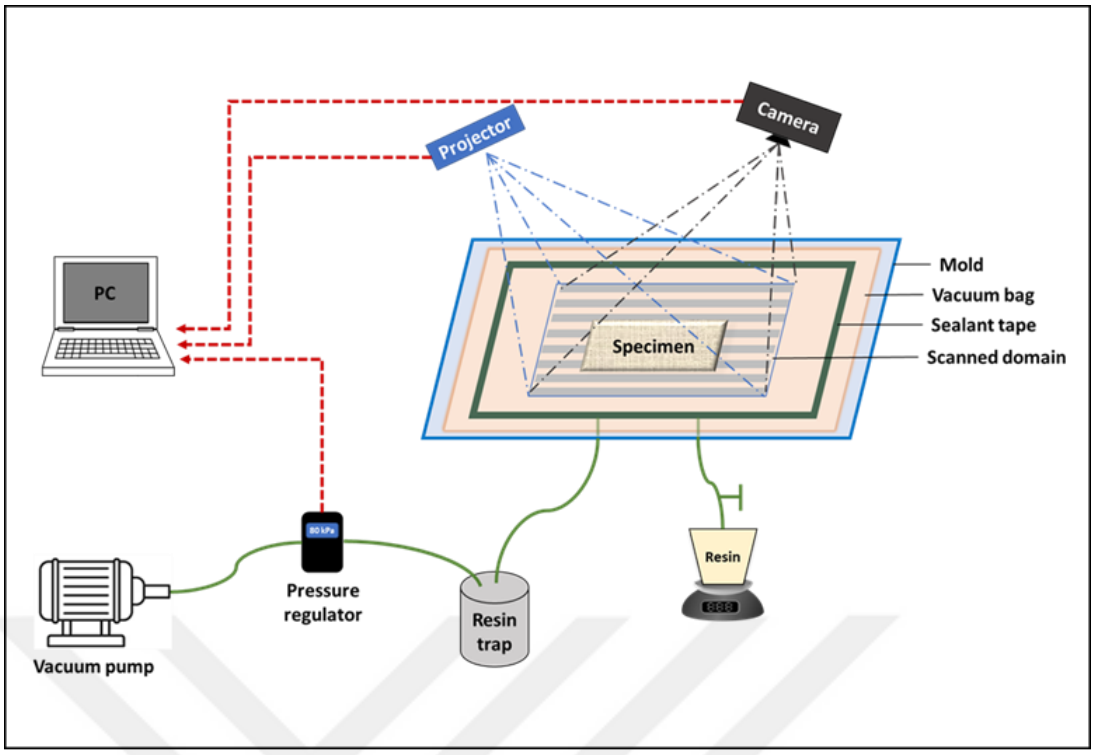

(a)

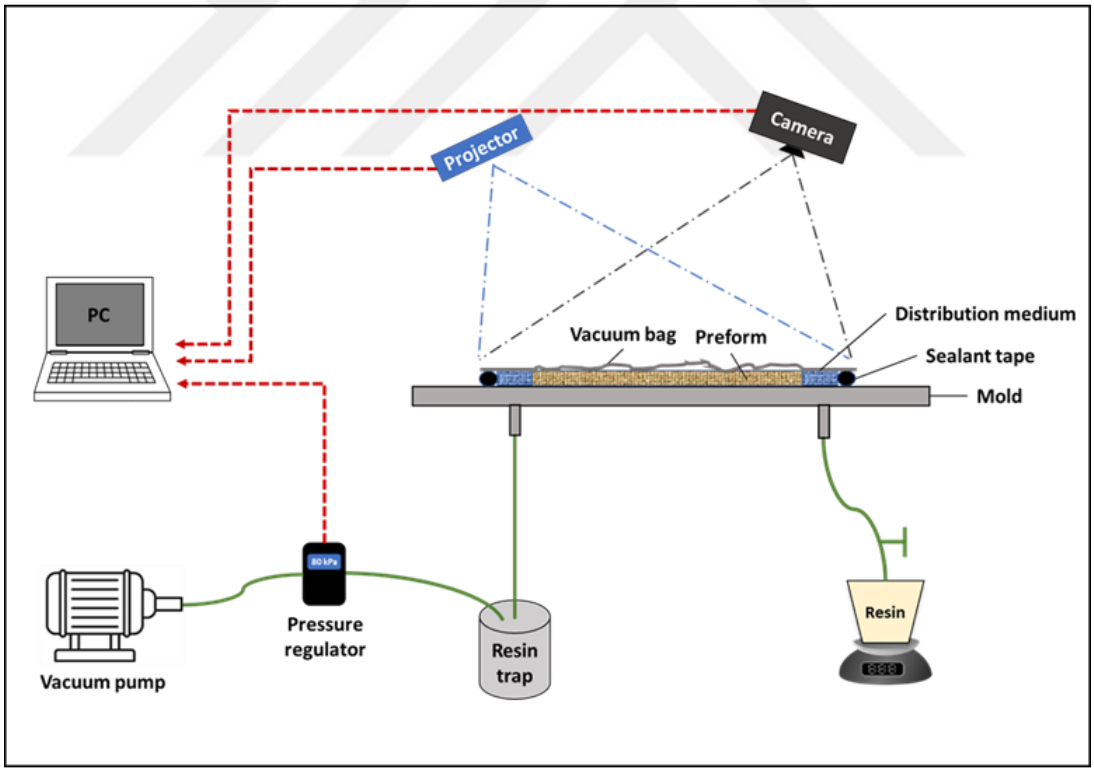

(b)

Figure 3.1: Vacuum Assisted Resin Transfer Molding (VARTM) experimental setup with thickness monitoring system (a) top view, (b) side view (adapted from Baris Caglar's PhD Thesis) [18].

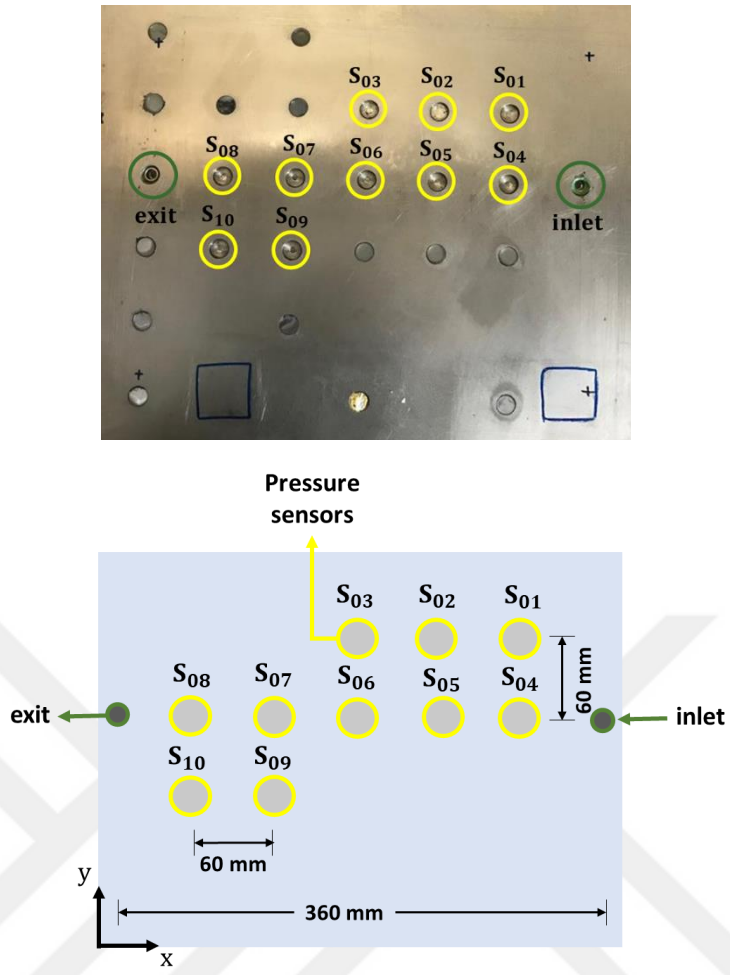

Figure 3.2: Flat mold with pressure sensors.

3.2 *1D Mold-Filling Experiment*

A flat mold is covered with a white tape as seen in Figure 3.3 to create a reference surface in the thickness monitoring system. Top of the 5 pressure sensors are not covered to monitor resin pressure during mold filling. These 5 sensors are underneath of the fabric preform in dimensions of 300x100 mm^2 along which 1D mold filling VARTM experiment are conducted. Flow mesh is placed at both inlet and exit to create 1D flow.

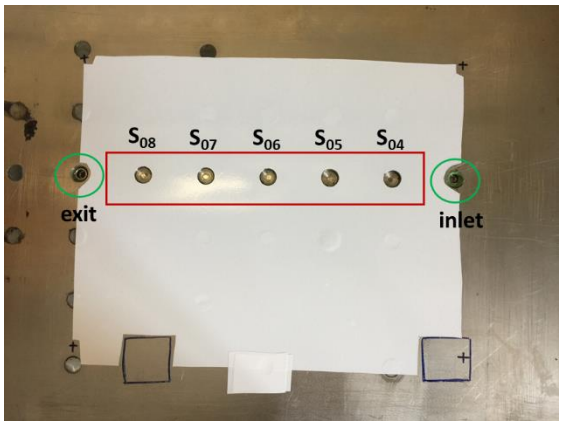

Figure 3.3: Flat mold for 1D mold-filling experiment.

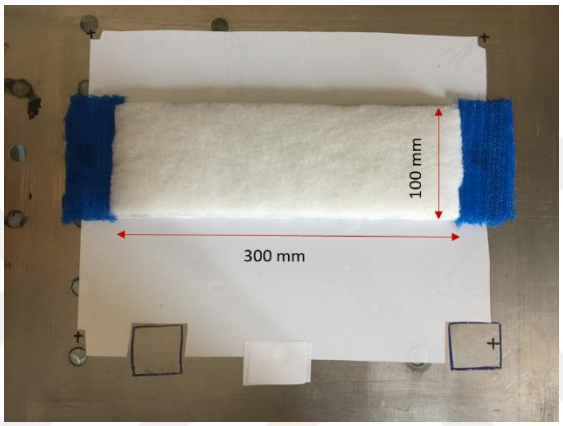

Figure 3.4: Preform and flow mesh placement.

3.2.1 Experimental Procedure

In 1D mold-filling experiment, one debulking cycle is accomplished at an increasing compaction pressure trend of 2, 5, 10, 20, 40, 60 kPa (by keeping the pressure at each of these values for 60 seconds) which is called loading or compaction stage, followed by a settling stage at 80 kPa for 5 min, followed by an unloading/decompaction stage (at a decreasing trend of 60, 40, 20, 10, 5 kPa), and finally a relaxation stage at 2 kPa for 5 min. Thickness scan is repeated twice, 30 and 60 seconds after compaction pressure is set to a particular level. Then, loading and settling sections are repeated. After settling at 80 kPa for 5 minutes injection is started by opening the resin inlet. During resin injection, scanning is repeated at every 10-second intervals. After the inlet is closed, scanning interval is increased to 15-seconds intervals. Figure 3.5 shows this experimental procedure.

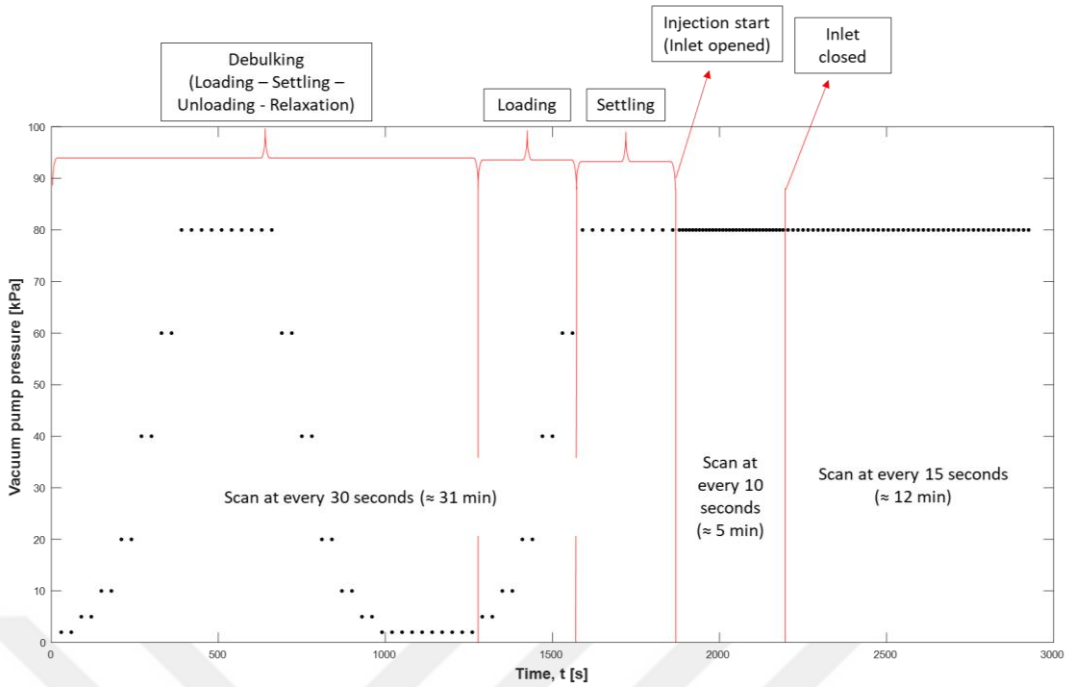

Figure 3.5: Controlling vacuum pressure at the exit side of the mold during a 1D Mold-filling experiment.

Figure 3.6 shows fiber preform dimensions. Blue regions (Region 1 and 2) are the selected core material area away from pressure sensors (and corresponding surface irregularities) where the thickness scanning data will be analyzed to determine the statistical variations (mean, standard deviation, maximum and minimum thicknesses).

3.2.2 Compaction Characterization

Compaction characterization relates thickness of fabric to the compaction pressure. Since fiber volume fraction is theoretically related to thickness, one can alternatively relate fiber volume fraction to compaction pressure by conducting compaction characterization experiments. In this study, test fabric preform material is in dry state which represents pre-impregnated fabric. Figure 3.7 shows the statistical variation of the thickness in the two blue regions (see Figure 3.6) versus time during a compaction cycle. As seen, thickness decreases while compaction pressure increases (loading) and vice versa for unloading. Also, compaction pressure kept constant at highest pressure level (80 kPa) for 5

minutes to achieve fiber settling. However, it is very noticeable that thickness varies with time at constant pressure (thicknesses at the beginning and at the end of the relaxation stage at 2 kPa) are very much different indicating that the material is not elastic, but viscoelastic. Thickness keeps varying with time during 80-kPa settling stage, too. Theoretical V_f is inversely proportional to thickness and calculated using $V_f = \frac{n\,\rho_{sup}}{\rho_f\,h}$. Figure 3.8 shows fiber volume fraction, V_f (h is the average thickness at the unloading stage) versus compaction pressure, P_c during unloading stage (between 660 and 1020 seconds in Figure 3.7) and the model fit. Compaction model constants, C and D in the exponential curve fit, $V_f = CP_c{}^D$ are computed by using the least square method. Model fit constants for upper and lower bounds (see Figure 3.8) are calculated to find standard deviation in model calculation as explained in detail in a further section. Fiber volume fraction increases from 8% approximately at minor load of 2 kPa to 20% approximately at the highest compaction pressure of 80 kPa.

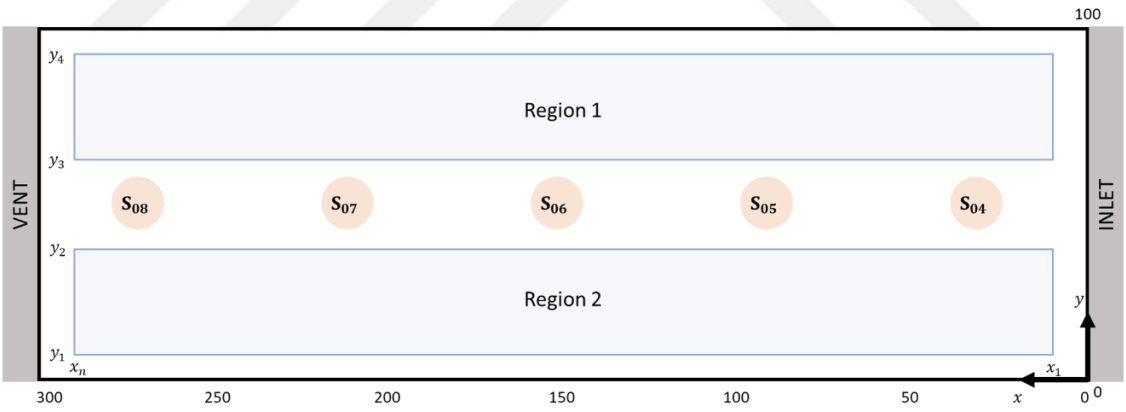

Figure 3.6: Average thickness is calculated by using the data from the two blue regions (Region 1 and Region 2) in VARTM compaction characterization experiments.

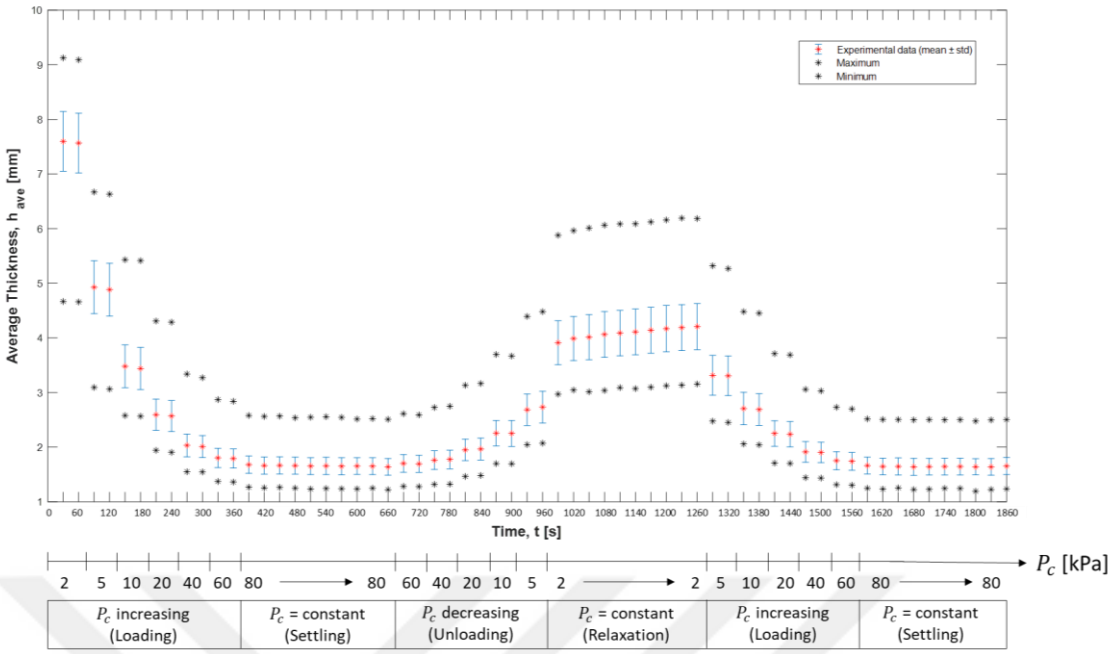

Figure 3.7: Average thickness of the two blue regions vs time during a compaction cycle.

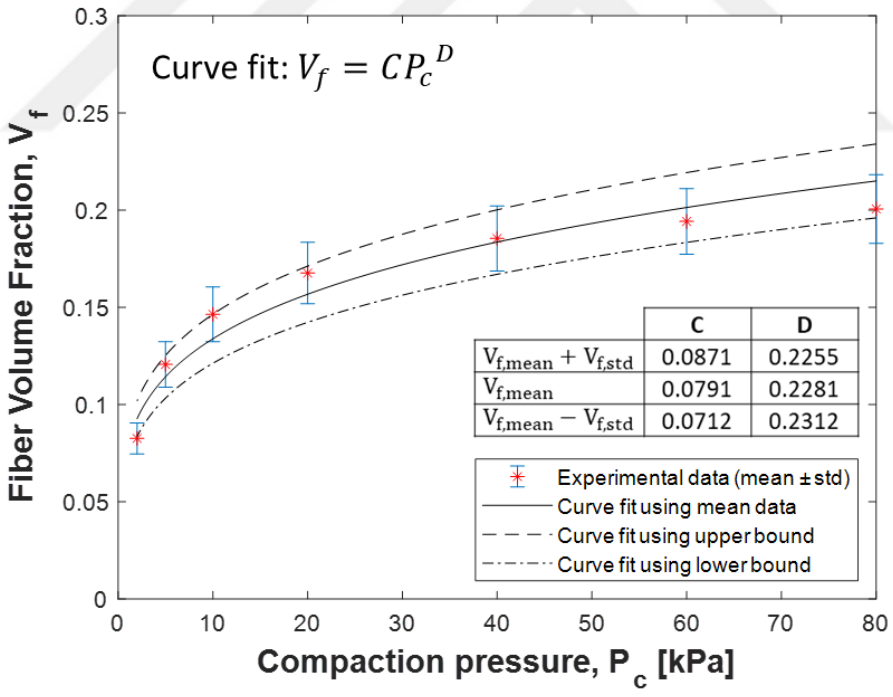

Figure 3.8: Compaction characterization experiment and the model fit.

3.2.3 Permeability Characterization

Resin flow front position is recorded every 10 seconds during core material filling. Unsaturated permeability, K_{uns} is calculated by using Eq. 3.1 [1] in which μ is viscosity

of resin, ϕ is porosity of preform which is calculated as $\phi = 1 - V_f$. Note that this Darcy assumption is based on a fixed thickness (h) which is satisfied in RTM, but not in VARTM due to flexible vacuum bag. While calculating theoretical V_f, h is taken as the average thickness of the latest 10 data (between t = 1590 s and 1860 s in Figure 3.7) at 80 kPa compaction pressure in compaction characterization experiment. Flow front position versus time data and its curve fit are presented in Figure 3.9. Unsaturated permeability is found as $K_{uns} = 2.96x10^{-10}$ m^2 (for the core material used in this study at h = 1.65 +/- 0.15 mm and V_f = 20 +/- 1.8% initially, i.e., just before the injection, and then became h = 1.89 +/- 0.35 mm and V_f = 18 +/- 3.0% at the end of the mold filling). The coefficient of determination, R^2 of permeability data is calculated using Eq. 3.2 where SS_{err} is the residual sum of squares and SS_{tot} is the total sum of squares. R^2 is determined as 0.9982. In general, coefficient of determination ranges between 0 and 1. If it is closer to 1, it means that deviation between data points and model is small [14].

After the mold filling (that means the resin reaches the vent and enough time is allowed for saturation, so that the preform is assumed fully saturated), saturated permeability, K_s is calculated by using Eq. 3. Here, resin mass data is used to find flow rate, and corresponding K_s is found as $2.93x10^{-10}$ m^2 (at h = 1.94 +/- 0.38 mm and V_f = 17 +/- 3.0%) with and R^2 is calculated as 0.9420.

$$x_f = \sqrt{\frac{2\,K\,\Delta P}{\mu\,\phi}\,t} \quad , \quad x_f = C\sqrt{t}$$
$$where\ \ C = \sqrt{\frac{2\,K\,\Delta P}{\mu\,\phi}}\ \ or\ \ K_{uns} = \frac{C^2\,\mu\,\phi}{2\,\Delta P} \tag{3.1}$$

$$R^2 = 1 - \frac{SS_{err}}{SS_{tot}}$$
$$where\ \ SS_{err} = \sum_i (y_i - f_i)^2\ \ and\ \ SS_{tot} = \sum_i (y_i - \bar{y})^2 \tag{3.2}$$

$$K_s = \frac{Q\,\mu\,L}{W\,h\,\Delta P}\ \ in\ [m^2] \tag{3.3}$$

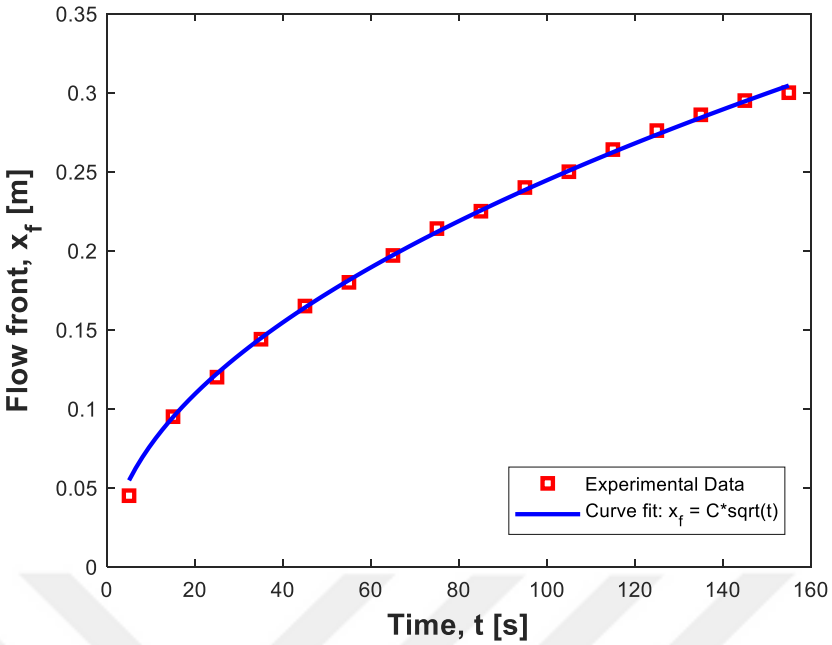

Figure 3.9: Flow front position versus time graph recorded during the unsaturated permeability measurement experiment with constant P_{in} boundary condition for the core material.

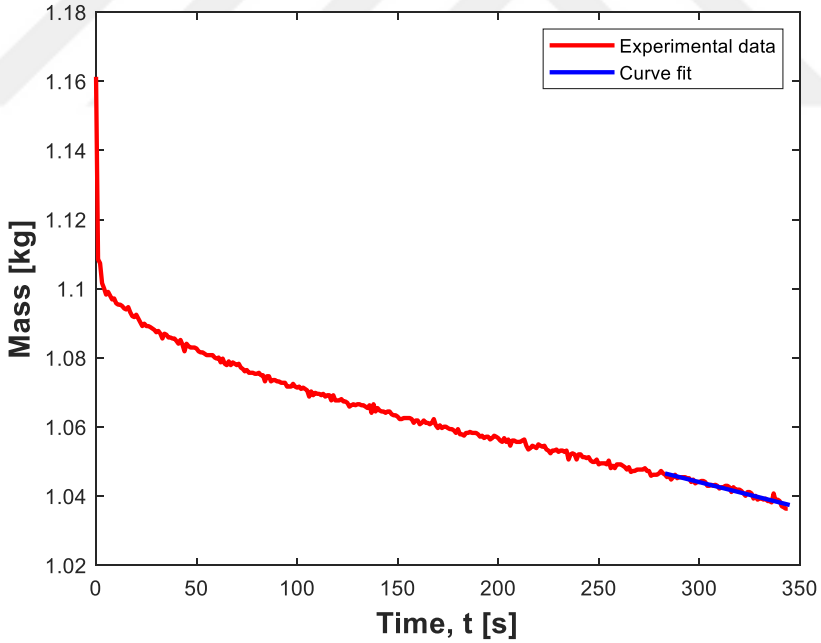

Figure 3.10: Mass of the silicon oil at the inlet during resin infusion.

3.2.4 1D Mold Filling

Figure 3.11 shows the average thickness along y (see Equation 3.4a) versus x direction for the fiber preform before resin infusion at P_c = 80 kPa. Thickness varies

between 1.78 mm (maximum) and 1.49 mm (minimum) with an average value of 1.65 mm and a standard deviation of 0.09 mm.

$$H(x,t) = \frac{1}{(y_2 - y_1) + (y_4 - y_3)} \left(\int_{y_1}^{y_2} h(x,y,t)dy + \int_{y_3}^{y_4} h(x,y,t)dy \right) \quad (3.4a)$$

$$h_{ave}(t) = \frac{1}{(x_2 - x_1)} \left(\int_{x_1}^{x_2} H(x,t)dx \right) \quad (3.4b)$$

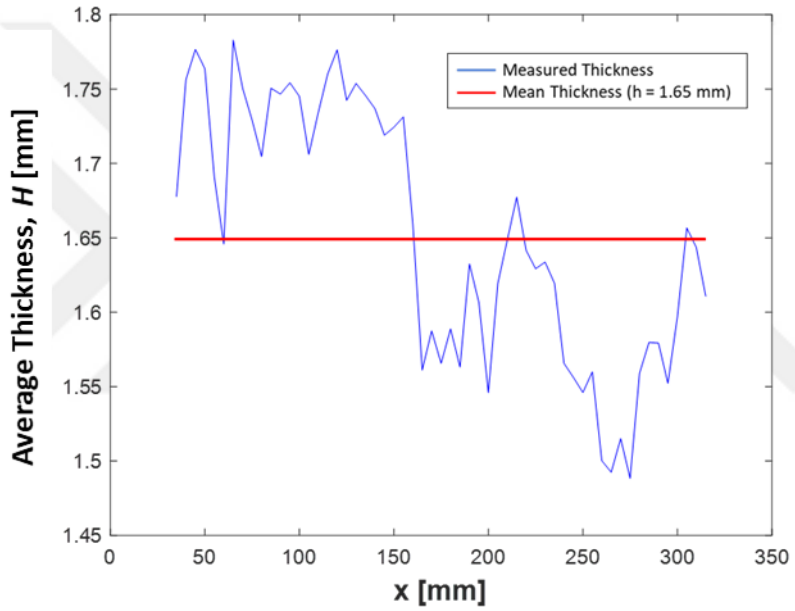

Figure 3.11: Average thickness versus x at 80 kPa compaction pressure and at t = 0 (just before the resin injection).

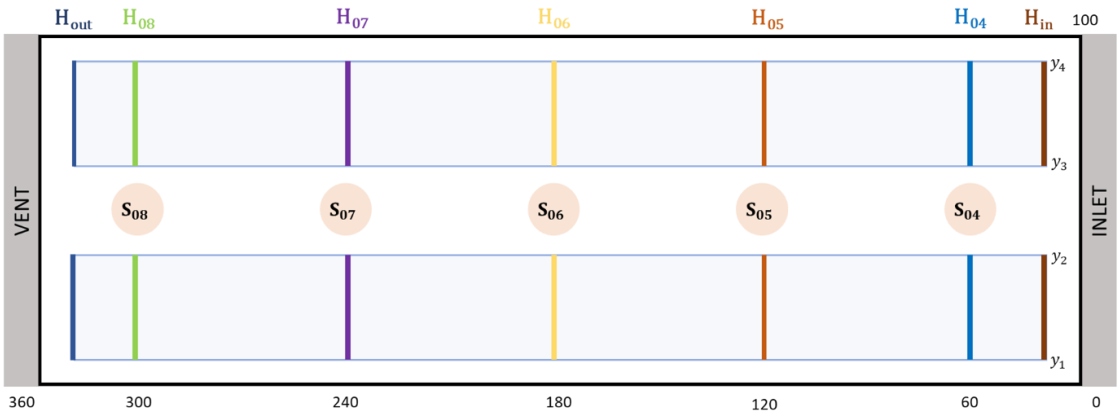

Figure 3.12: Sensor locations and measured thickness locations.

Scanning is achieved every 10 seconds during mold filling. Thickness values that are used in average thickness calculation during mold filling are illustrated with colored lines at five pressure sensor ($H_{04}, H_{05}, H_{06}, H_{07}, H_{08}$) location and inlet and exit (H_{in}, H_{out}) in Figure 3.12. $H_{in}, H_{04}, H_{05}, H_{06}, H_{07}, H_{08}, H_{out}$ (from right to left) are located at 35, 60, 120, 180, 240, 300, 315 mm away from the inlet, respectively. Figure 3.13 shows thickness distribution at five different instants (t = t_{fill}, t_{fill}+30 s, $t_{injclosed}$, $t_{injclosed}$+60 s and $t_{end} = t_{1000}$) to see the settlement of thickness with time. Each red star represents the mean (average) of 14 nodal points (7 nodes in Region 1, and 7 nodes in Region 2 as seen in Figure 3.6) along each $H_{0\#}$, each blue bar represents the standard deviation and two black stars per $H_{0\#}$ are the maximum and minimum values. Fiber volume fraction, V_f is calculated using the theoretical formula $V_f = \frac{n\,\rho_{sup}}{\rho_f\,h}$.

Resin flow starts by opening the inlet, and immediately the thickness starts increasing with time in the resin-filled region since the upper mold is a flexible vacuum bag. Thickness gets the maximum value near the inlet (H_{in}) at t = $t_{fill.}$ It keeps increasing with time as long as the inlet and exit are open. When the inlet is closed, but the exit is still open, resin pressure near the inlet decreases and thus the compaction pressure increases with time. Pressure settling (and thus thickness settling) is not immediate or very fast, it takes some time in the order of minutes to hours depending on the part size. As seen in Figure 3.13 after the injection is closed, thickness of the fiber preform at specified locations starts decreasing and then almost settle. At t = t_{end}, average thickness of the 7 location is 1.66 mm (maximum and minimum thicknesses are 1.82 and 1.56 mm, respectively) with a standard deviation of 0.09 mm, and the corresponding fiber volume fraction is between 18 and 21%.

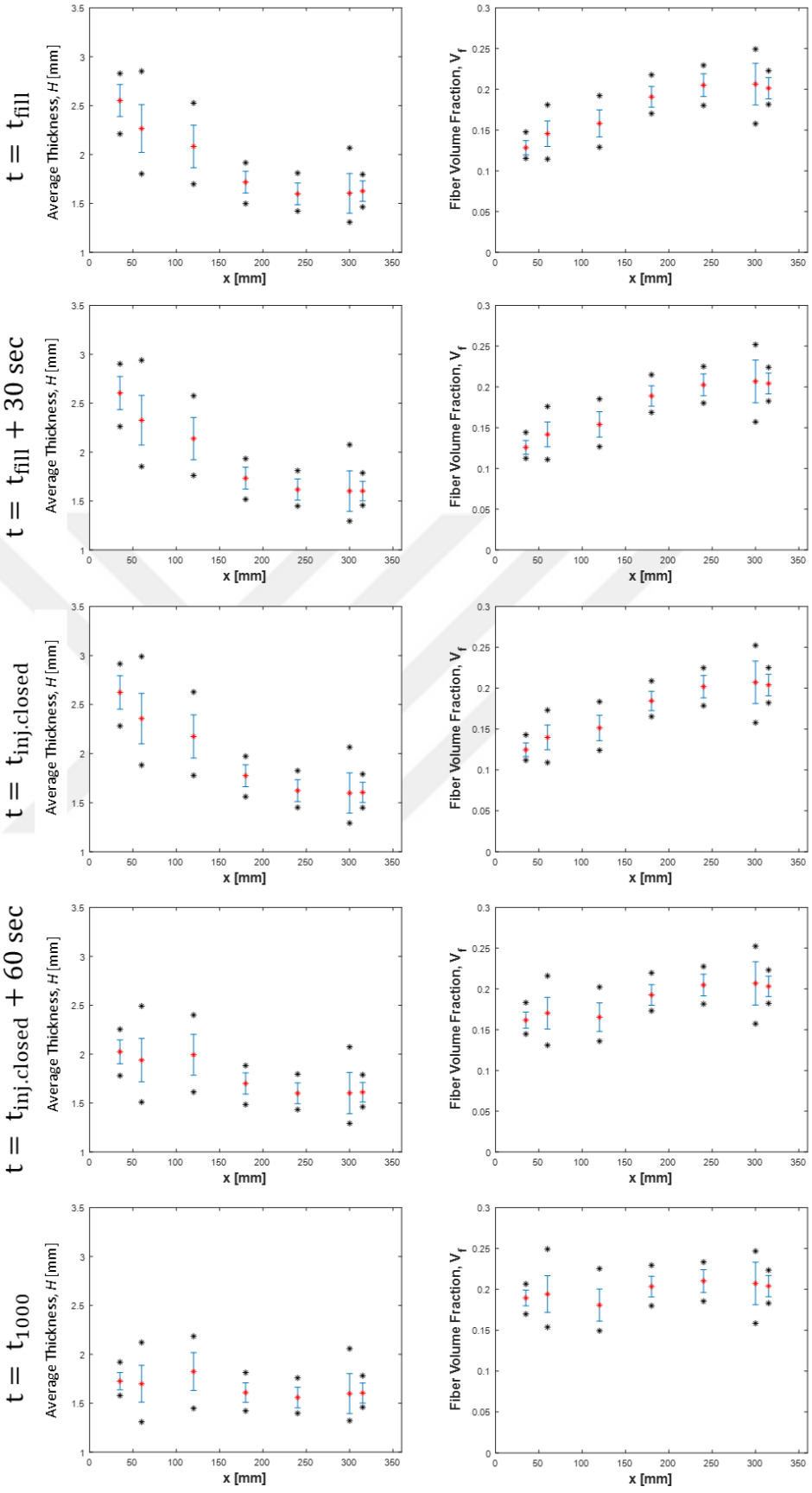

Figure 3.13: Experimental average thickness (with standard deviation, maximum and minimum) values and calculated V_f at specified sensor locations.

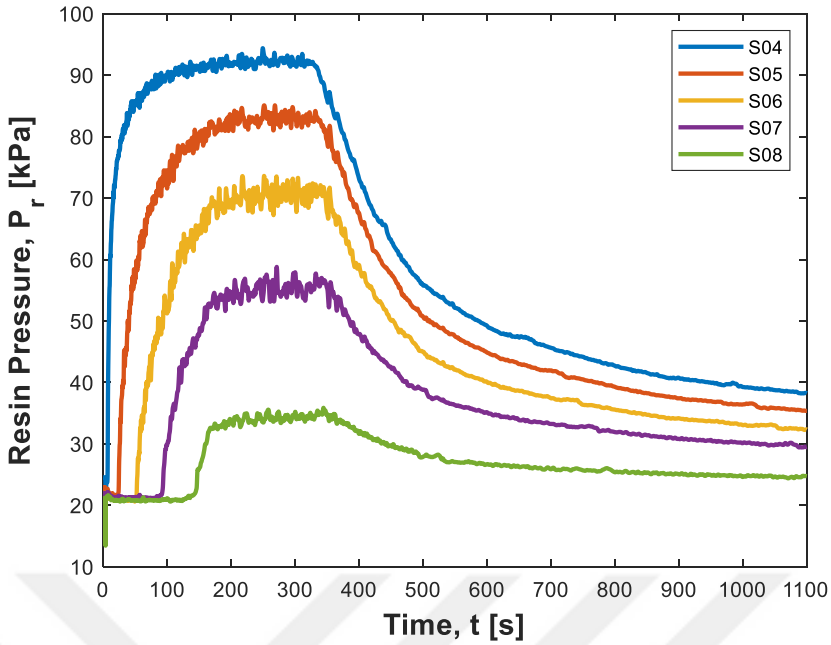

Figure 3.14: Resin pressure versus time graph for five pressure sensors.

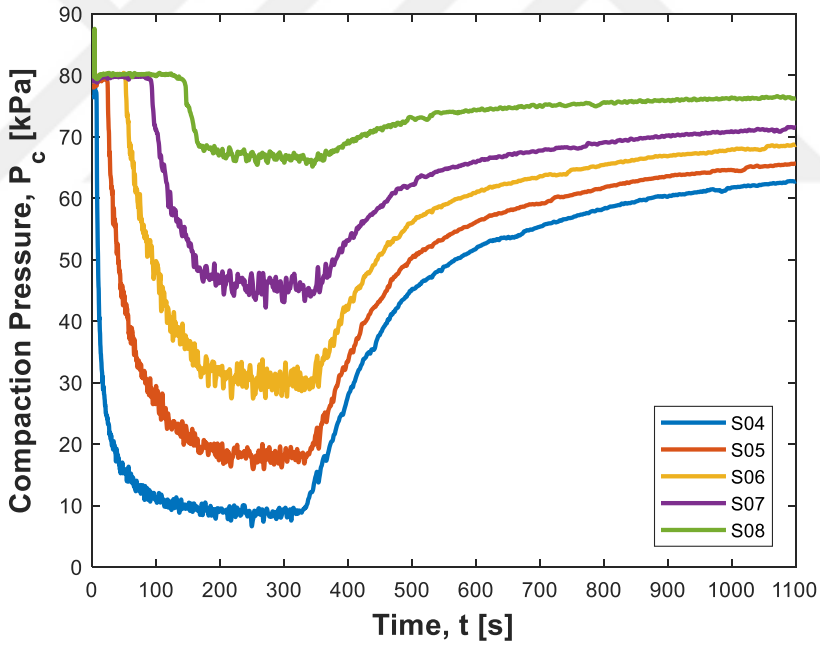

Figure 3.15: Compaction pressure versus time graph for five pressure sensors.

Resin pressure is measured using pressure sensors ($S_{04}, S_{05}, S_{06}, S_{07}, S_{08}$) at x = 60, 120, 180, 240 and 300 mm away from the line inlet. Figures 3.14 and 3.15 show resin pressure versus time and compaction pressure versus time graphs for five pressure sensors, respectively. Resin pressures (gage, i.e., relative to atmospheric) for the inlet is calculated using $\Delta P = \rho\, g\, z$ where z is the elevation between the mold and resin inlet, and ρ and g are the resin density and gravitational acceleration, respectively. Similarly,

resin pressures (gage, i.e., relative to vacuum pressure at the vacuum pump) for the exit is calculated using $\Delta P = \rho\ g\ z$ where *z* is the elevation between the mold and resin trap. Compaction pressure is calculated using $P_c = P_{atm} - P_r$ (see Figure 3.15) when the fabric is saturated with resin. V_f is calculated using a power law empirical relationship, $V_f = CP_c^{\ D}$, where the model constants C and D were already calculated earlier (see Figure 3.8). h is calculated using theoretical relationship: $h = \frac{n\ \rho_{sup}}{\rho_f V_f}$ (see Figure 3.16). Standard deviation of V_f is calculated using power law formula and shown in Figure 3.8. Standard deviation of simulated h is computed using $h_{std} = \frac{\left(\frac{n\ \rho_{sup}}{\rho_f (V_{f,mean} + V_{f,std})}\right) - \left(\frac{n\ \rho_{sup}}{\rho_f (V_{f,mean} - V_{f,std})}\right)}{2}$. For the model constants and statistical variations, see Figure 3.8. After the injection gate is closed, simulated thickness starts decreasing and then almost settle similar to experiment results. As resin pressures at the inlet and exit are calculated using $\Delta P = \rho\ g\ z$ formula (which do not vary with time), simulated thickness and hence fiber volume fraction are constant at these locations. Because of that reason, after the injection is closed, thickness at the inlet (H_{in}) is not shown in Figure 3.16 at t = $t_{injclosed}$+60 s and t_{end}.

When the experiment and model results are compared, average of the experimental thickness at t = t_{end} seconds is around 4% higher from the model.

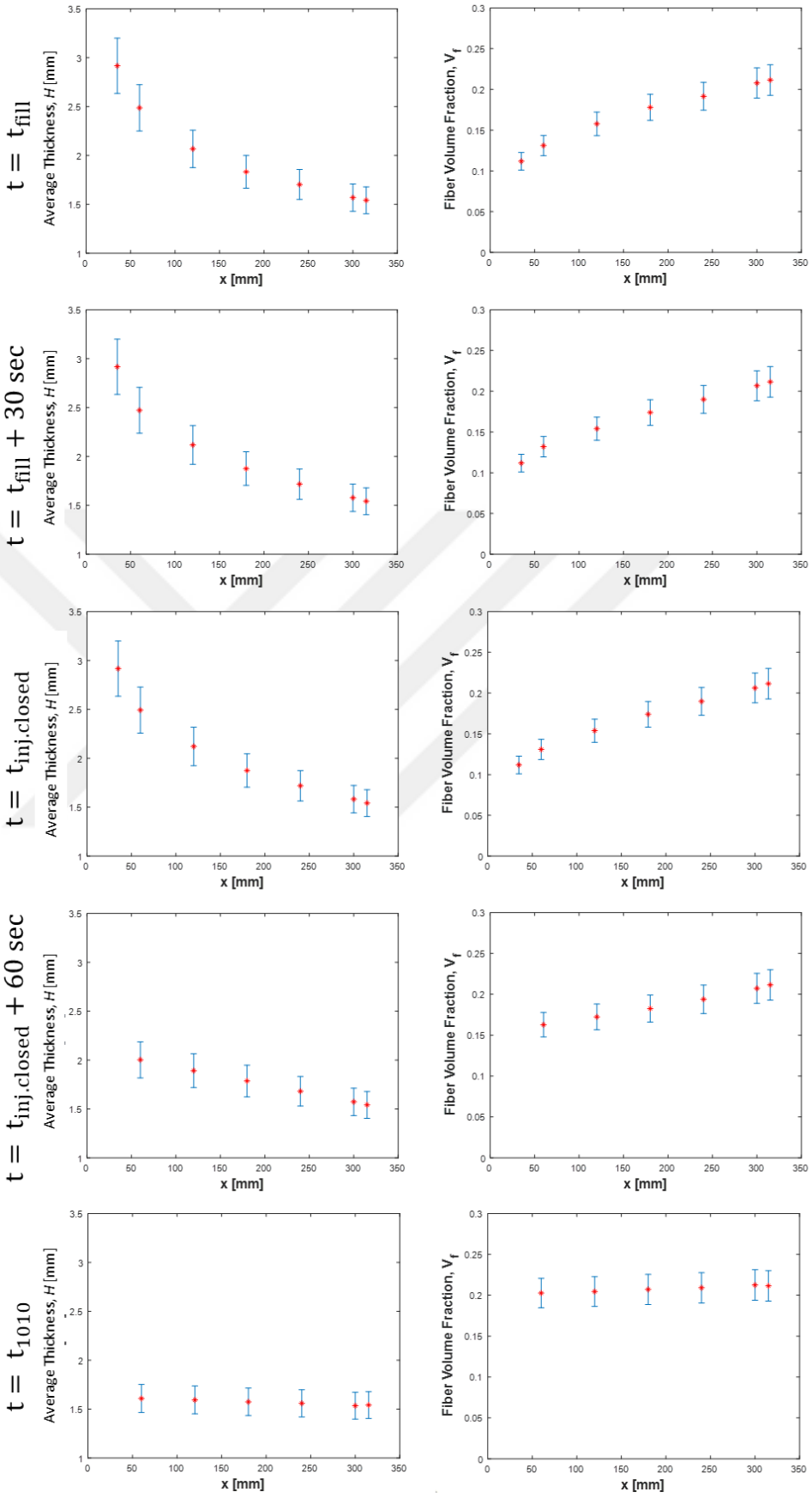

Figure 3.16: Simulated average thickness and fiber volume fraction for 1D case.

Figure 3.17 compares experimental and simulated (model) thicknesses. Thickness starts to increase near inlet because of the non-rigid vacuum bag after resin injection. When injection is closed, thickness settles and reaches a steady value if spend sufficient time.

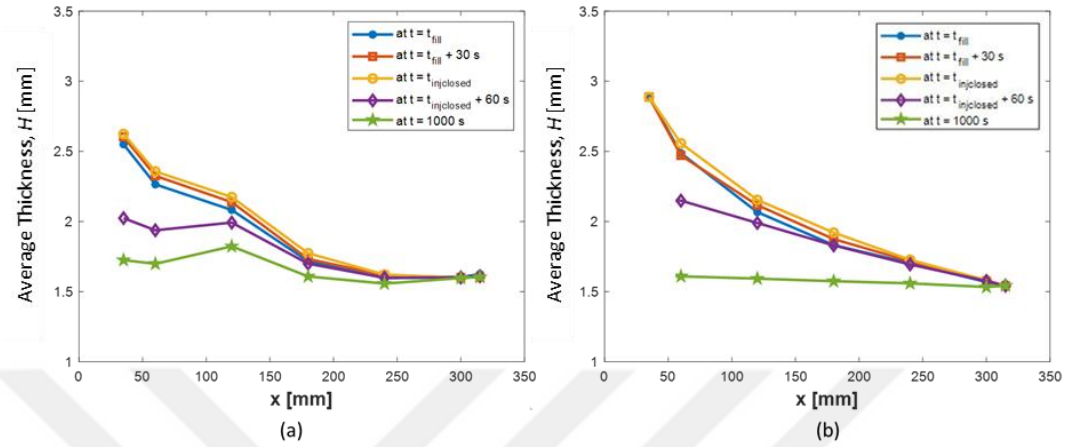

Figure 3.17: Thickness as a function of location and time: (a) experimental, (b) model.

Table 3.1: Experimental and modeled thicknesses and fiber volume fraction values at sensor locations at t = t_{end} (std stands for standard deviation and thicknesses are in mm).

			H_{in}	H_{04}	H_{05}	H_{06}	H_{07}	H_{08}	H_{out}
Experiment	H	mean	1.73	1.70	1.82	1.61	1.56	1.60	1.60
		std	0.09	0.19	0.19	0.10	0.11	0.20	0.10
	V_f	mean	0.19	0.19	0.18	0.20	0.21	0.21	0.20
		std	0.01	0.02	0.02	0.01	0.02	0.03	0.01
Model	H	mean	-	1.61	1.59	1.57	1.56	1.53	1.54
		std	-	0.14	0.14	0.14	0.14	0.14	0.14
	V_f	mean	-	0.20	0.20	0.21	0.21	0.21	0.21
		std	-	0.02	0.02	0.02	0.02	0.02	0.02

3.3 2D Mold-Filling Experiment

In a 2D mold-filling experiment, 10 pressure sensors are used to monitor resin pressure; and SLS system is used for full-field thickness monitoring. Placement of two layers of fabric preform (i.e., core material in white region), and flow mesh (i.e.,

distribution medium in blue color) can be seen in Figure 3.18. Dimensions of the core material for 2D mold filing VARTM experiment can be seen in Figure 3.19.

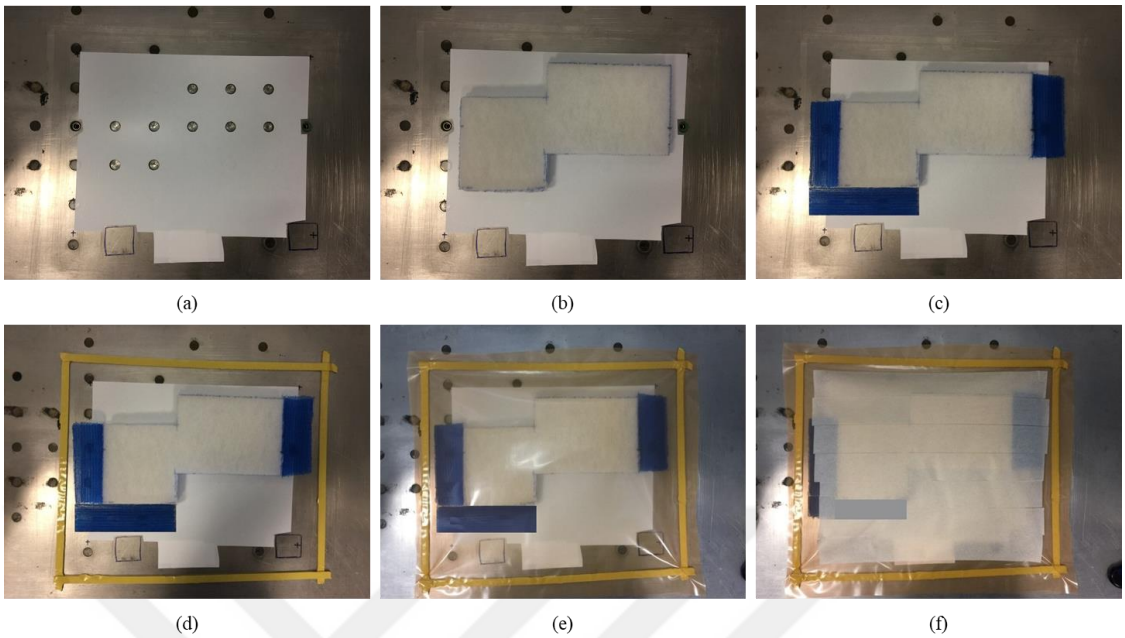

Figure 3.18: Preform and flow mesh placement.

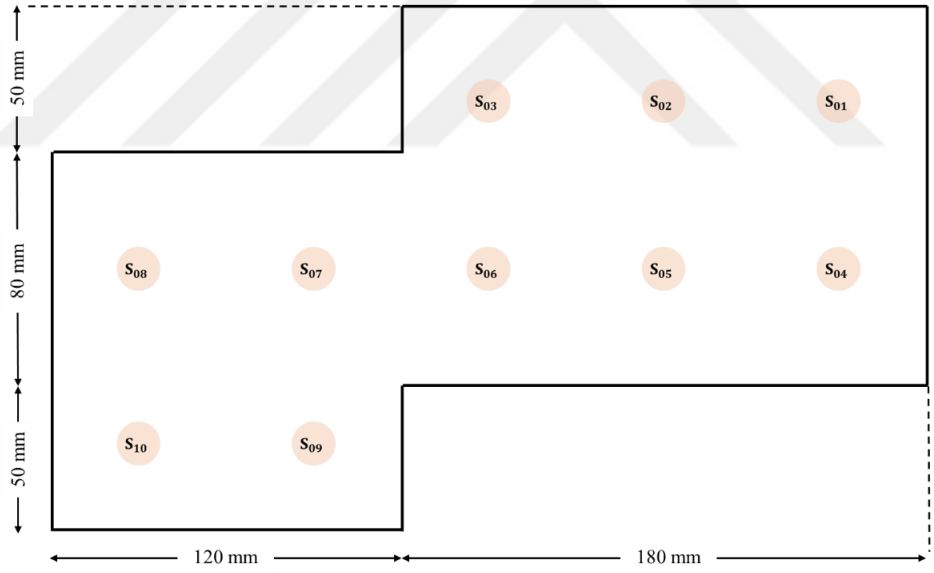

Figure 3.19: Dimensions of the core material for 2D mold filling experiment.

3.3.1 Compaction Characterization

Experimental procedure for compaction characterization of 2D experiment is the same as 1D experiment. One debulking cycle is accomplished as a combination of loading, settling, unloading and relaxation stages. After this debulking, loading stage and settling stage (at 80 kPa for 5 minutes to settle the fiber preform) is repeated. Figure 3.20 shows the selected area (blue region) on the core material which is outside of the pressure

sensors (and thus excluded from the corresponding surface irregularities induced by the surface indentation near these sensors). The thickness scanning data is analyzed in these regions to determine the statistical variation (mean, standard deviation, maximum and minimum values) of the thickness versus time data during a compaction cycle as seen in Figure 3.21. Fiber volume fraction is calculated as approximately 22% with a standard deviation of 2.45% at 80 kPa compaction pressure just before unloading stage in compaction characterization. Fiber volume fraction, V_f versus compaction pressure, P_c during unloading stage (between 660 and 1020 seconds in Figure 3.21) and the model fit can be seen in Figure 3.22 with compaction model constants C and D calculated as 0.0784 and 0.2551, respectively.

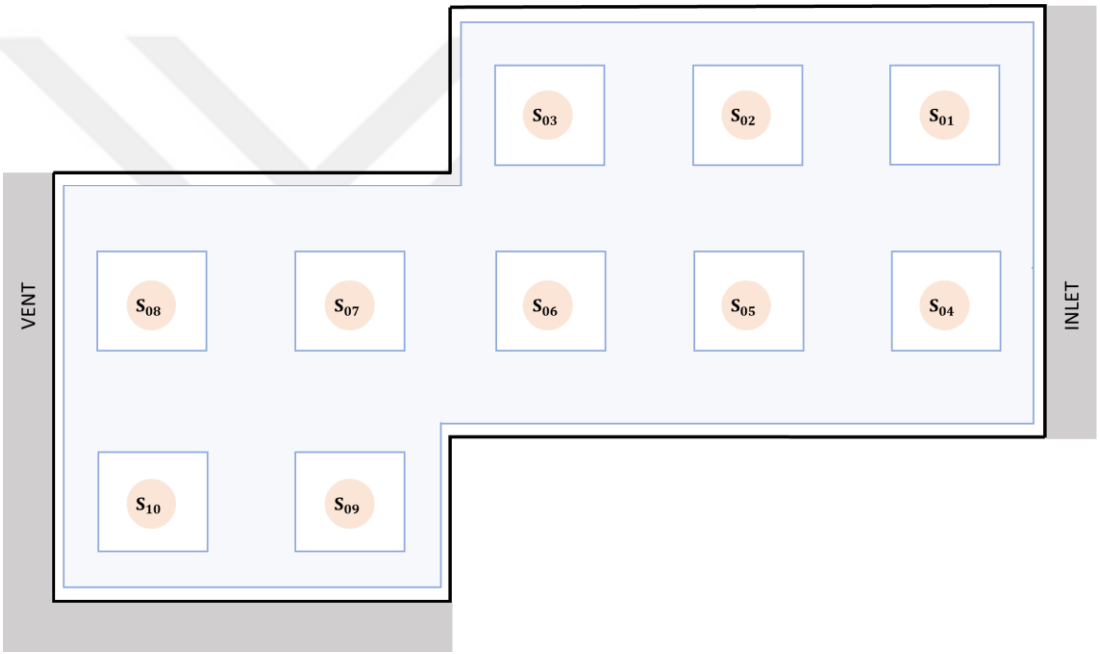

Figure 3.20: The scanned thickness data in the blue region only is used to exclude surface irregularity induced by the ten pressure sensors.

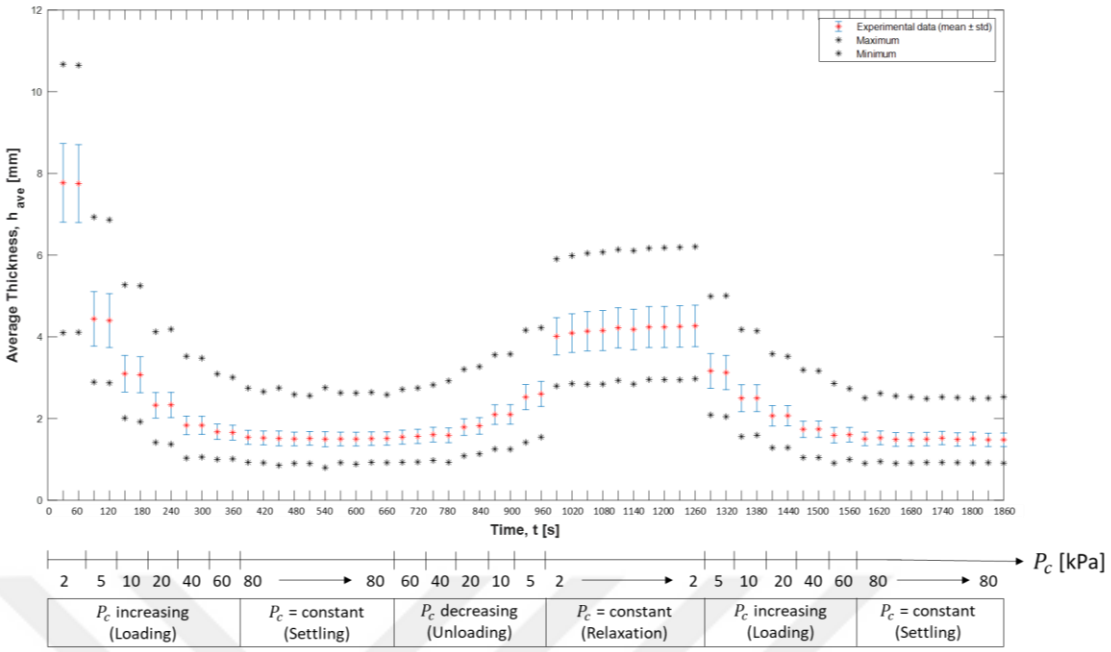

Figure 3.21: Average thickness (of the blue region in Figure 3.20) versus time during a compaction cycle.

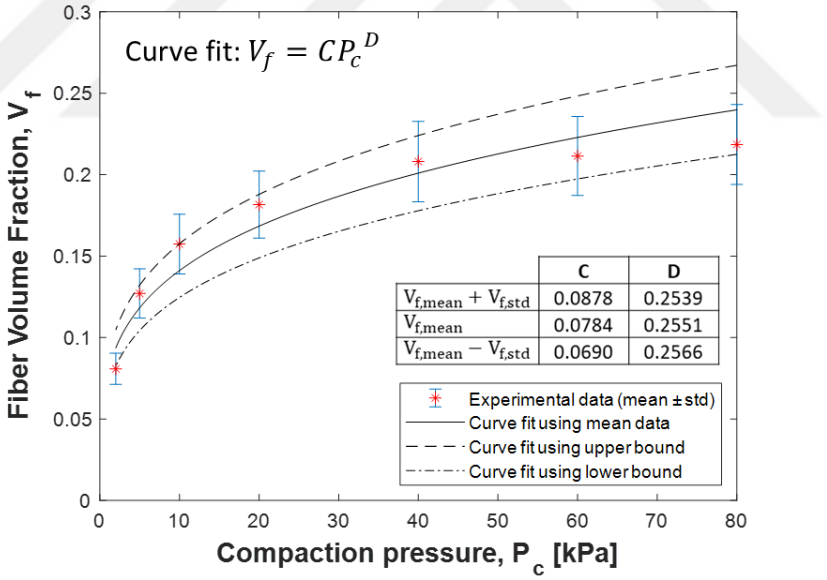

Figure 3.22: Compaction characterization experiment during unloading stage and the model fit.

3.3.2 2D Mold Filling

After compaction characterization of the preform, mold filling is started by opening the inlet and resin flow. Thickness distribution is recorded every 10 seconds during the mold filling and continued resin flush which takes approximately 5 minutes. After the inlet is closed but ventilation is kept continued scanning interval is increased to 15-second

intervals. Figure 3.23 shows the illustration of dummy fabric preform (core material) and flow meshes, and blue square edges around sensors used for thickness calculation during the mold filling. Along the edges of each of these blue squares which is outside of a sensor, surface irregularity induced by sensor placement rings will be eliminated in the thickness monitoring. In each of these blue square edges, there are 24 nodal points of SLS system used; and the statistical variation (average and standard deviation) of these 24-thickness data will be monitored. Figure 3.24 shows the average thickness distribution of the fiber preform before resin infusion at 80 kPa compaction pressure. For this experiment, H varies between 1.34 and 1.60 mm with a standard deviation of 0.08 mm. Figure 3.25 shows the flow front position at every scan time (with an interval of 10 seconds). Flow front position is recorded using a video camera which is placed on top of the preform. Core material is completely wetted at t = 225 seconds approximately. The inlet is closed around t = 310 seconds. Figure 3.26 shows the average thickness, H (average of 24 nodal points on blue square edges around each sensor, each square) versus time graph during resin infusion. As seen from that figure, there is a sudden decrease in thickness when the injection is closed (around t = 310 seconds). Thickness monitoring is continued until around t = 600 seconds with an interval of 15 seconds after the injection is closed. Thickness starts decreasing and eventually settle after the injection is closed. Initial thickness (at t = 0) in Figure 3.26 is the thickness just before the beginning of the resin infusion. As seen, thickness variation exists because of the inherent irregularities of preform surface induced by fiber structure nonuniformity as well as fabric cutting and placement. However, notice that the dummy fabric used here (core material) is expected to have much smaller irregularity compared to typical actual fabric preforms used in LCM. Also, thickness monitoring system's accuracy contributes to these variations. Locations of the SLS nodes may shift with time (i.e., between the scannings), or a slight change in the dynamically varying surface may cause shift of these points on the wrinkled vacuum bag, and thus they all contribute to the inaccuracy (see *Accuracy of the SLS System* part in Chapter 1). Figure 3.27 shows change in thickness, ΔH (i.e., $H(x,t) - H(x,0)$) versus time graph.

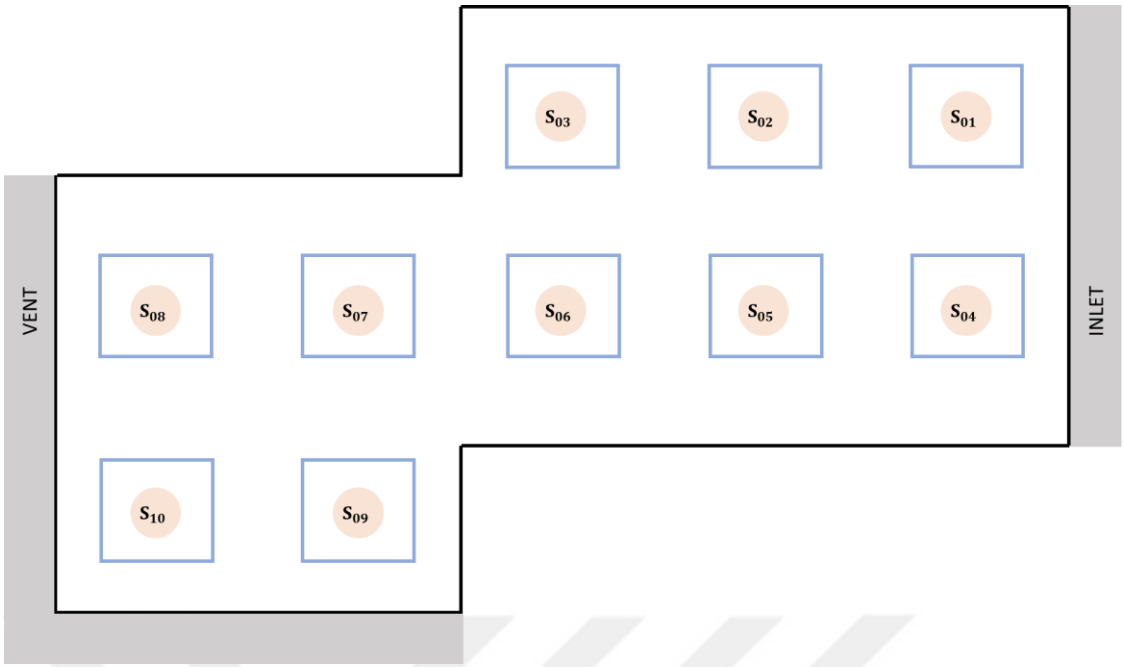

Figure 3.23: Edges of a blue square around each sensor where the scanned thickness values is used to calculate the average thickness, *H*.

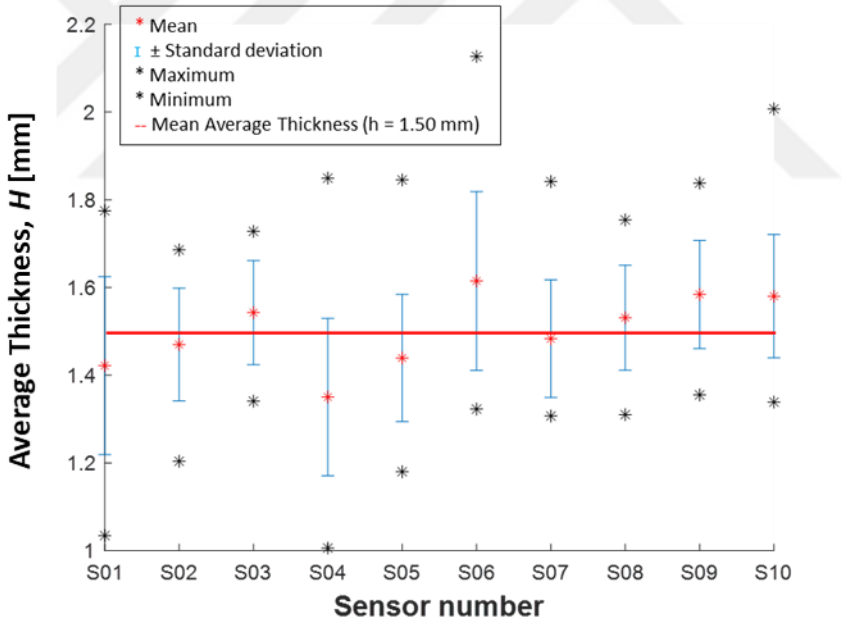

Figure 3.24: Average thickness of blue square edges (see Figure 3.23) for the ten pressure sensors before resin injection (at $P_c = 80$ kPa).

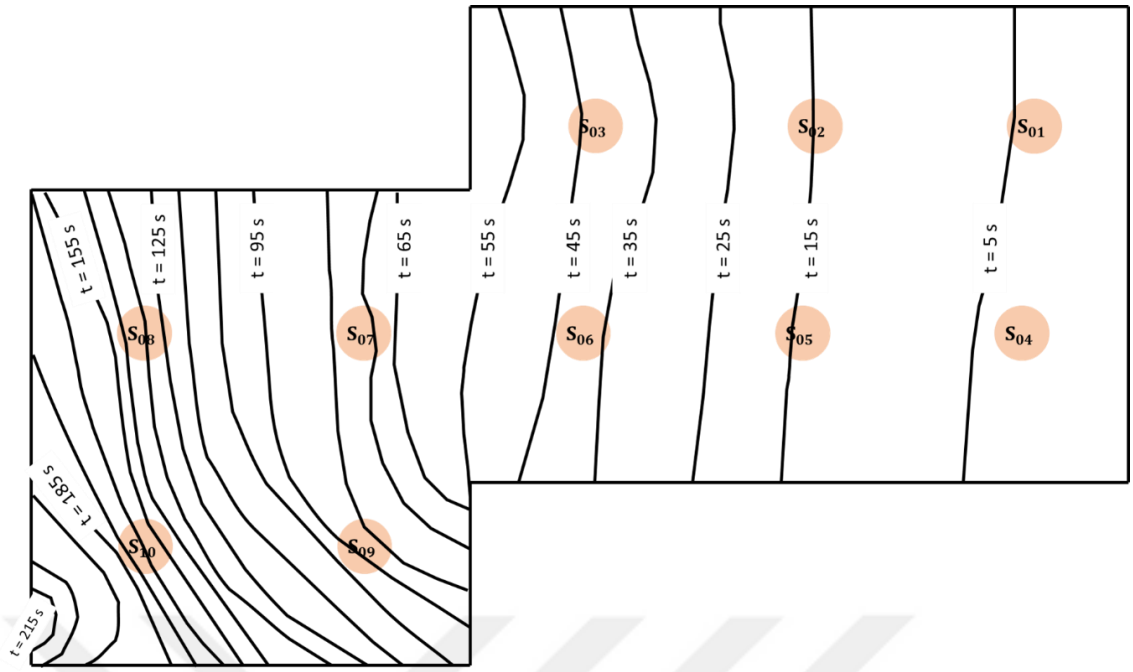

Figure 3.25: Flow front position at different instants for the 2D mold filling experiment.

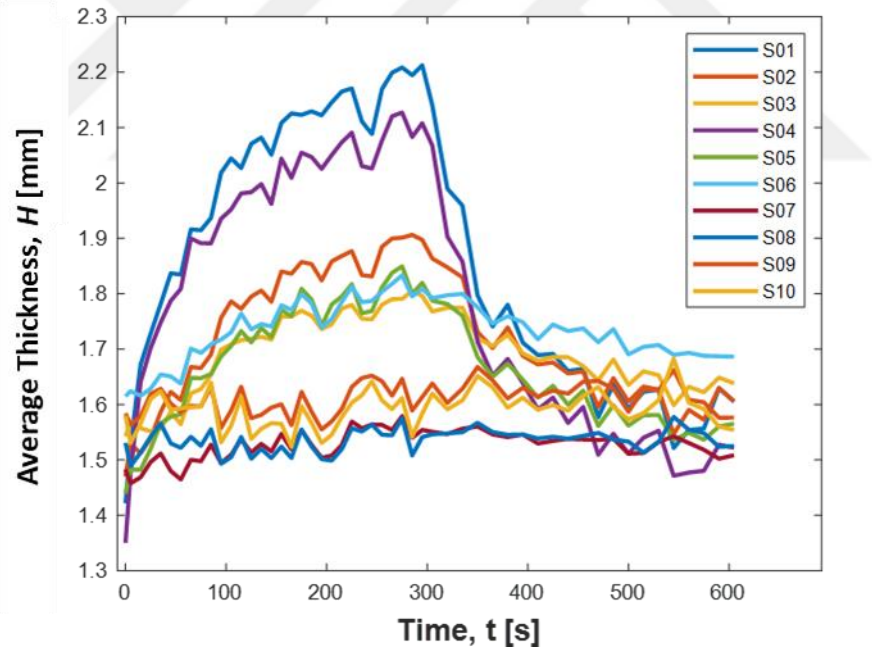

Figure 3.26: Experimental average thickness versus time graph after resin infusion.

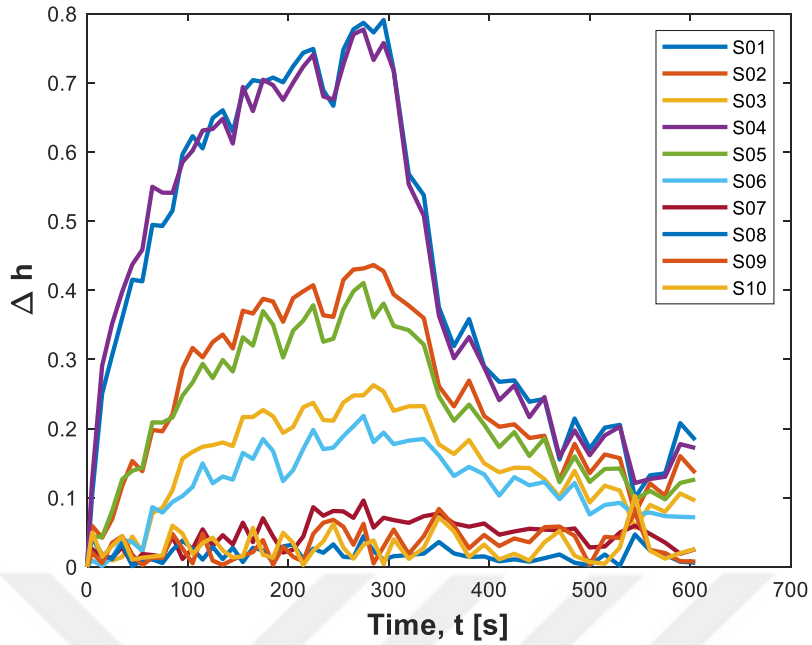

Figure 3.27: Experimental Δh versus time graph during mold filling ($0 < t < 310\ s$) and post-filling ($310\ s < t$).

Resin pressure is recorded after resin injection is started. Figure 3.28 shows resin pressure versus time graph for 10 pressure sensors. First, resin arrives at the closest sensors which are sensor numbers 1 and 4, followed by 5, 2, 3, 6, 7, 9, 8 and 10th sensors.

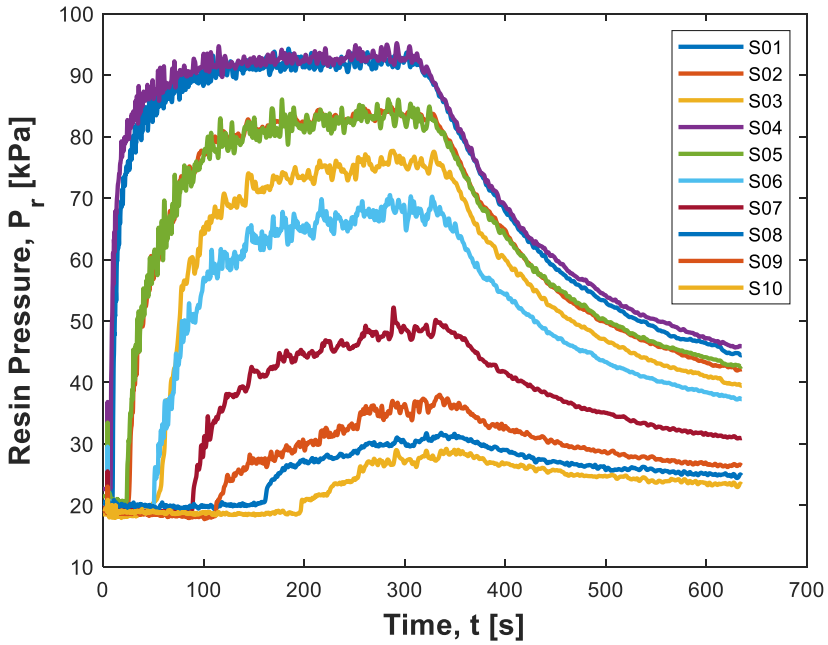

Figure 3.28: Resin pressure versus time graph for ten pressure sensors.

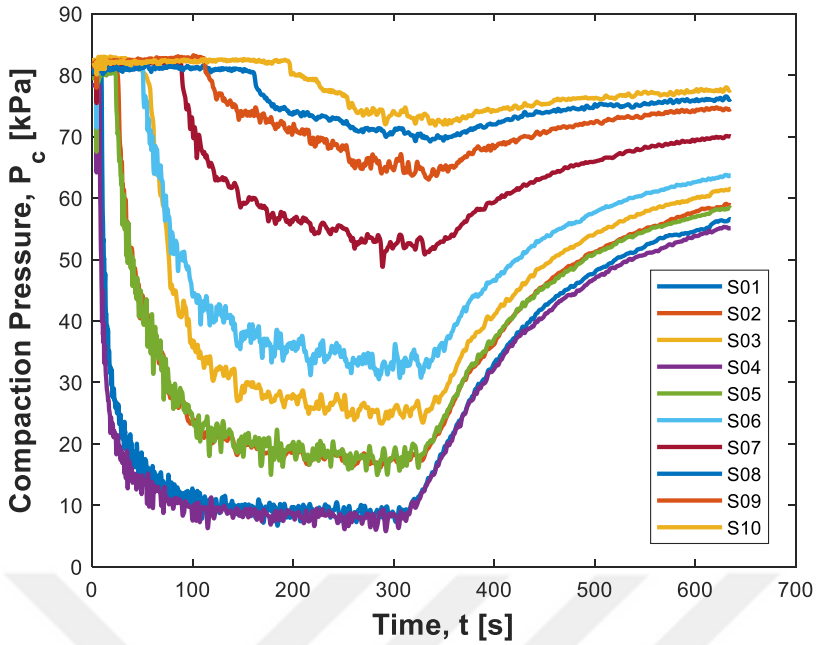

Figure 3.29: Compaction pressure versus time graph for ten pressure sensors.

In LCM processes, reinforcement material should be completely filled with matrix component (liquid polymeric resin). Incomplete mold filling causes some defects (decrease in mechanical properties and endurance against environmental conditions) affecting the quality of manufactured part. Modeling of resin pressure and fabric compaction helps us to investigate the resin impregnation process and the part thickness distribution. It allows us to take appropriate control actions so that parts are manufactıred without dry spots. As resin (fluid) flows through fabric preform (porous medium) during mold filling in VARTM, it can be modeled using Darcy's law. VARTM process is often used to manufacture complex and large-scale composite parts which requires longer processing and filling times, so it is very advantegous to model flow through fabric in VARTM process so that the part quality is enhanced.

In this thesis, steady state pressure and velocity distributions are modeled at the end of mold filling (i.e., when the mold is completely filled). The differential equation is obtained by substituting Darcy velocity components in the conservation of mass. The boundary conditions are as follows: (1) no leakage and thus no normal velocity component at the mold wall; and (2) injection resin pressure is known at the inlet and exit gates. Pressure distribution is solved by using Finite Difference Method (FDM). Discretized mold cavity is illustrated in Figure 3.30 and it depicts all the boundary conditions on the edges and governing differential equations within the mold cavity.

Silicon oil is supplied as a line source (using flow mesh) to impregnate the preform in the mold. It enters from the right edge shown with empty black circles on red line and it leaves the preform from left and bottom edges shown with empty black circles on blue line (see Figure 3.30). Modeling is done by using RTM assumption in which the mold thickness do not vary with time. However, in VARTM process, non-constant mold gap (i.e., part thickness) deviates from RTM condition due to the flexible vacuum bag used as upper mold. A more accurate modeling can be done by assigning thickness to each element of FEM and updating it after each time step. Here, instead of FEM, FDM will be used, and initial thickness will not be updated. This will bring some inaccuracy induced by dimensional change, however a straightforward and quick modeling is achieved. Thickness of the cavity is taken as 1.79 mm (average of the 24x10 = 240 nodes, i.e. 24 nodes around each sensor, and a total of 10 sensors seen in Figure 3.23) for the last 60 seconds just before resin inlet is closed).

Conservation of mass equation for the incompresible (ρ = constant) and steady flow is written as [1]

$$\nabla . \boldsymbol{U} = 0$$

$$\frac{\partial u}{\partial x} + \frac{\partial v}{\partial y} = 0$$

$$\frac{\partial}{\partial x}\left(-\frac{K_{xx}}{\mu}\frac{\partial P}{\partial x}\right) + \frac{\partial}{\partial y}\left(-\frac{K_{yy}}{\mu}\frac{\partial P}{\partial x}\right) = 0$$

$$K_{xx}\frac{\partial^2 P}{\partial x^2} + K_{yy}\frac{\partial^2 P}{\partial y^2} = 0 \qquad (3.5)$$

Velocity components are written using Darcy's Law: $u = -\frac{K_{xx}}{\mu}\frac{\partial P}{\partial x}$ and $v = -\frac{K_{yy}}{\mu}\frac{\partial P}{\partial y}$.

Assuming that fabric material is isotropic and thus permeability is constant in all in-plane directions: $K_{xx} = K_{yy} \equiv K$, the differential equations is simplified as the classical Laplace equation:

$$\frac{\partial^2 P}{\partial x^2} + \frac{\partial^2 P}{\partial y^2} = 0 \qquad (3.6)$$

This is a well suited assumption for the core material used here due to its isotropic structure.

All boundary conditions are given below:

B.C at left upper edge, (x,y) = (0-0.12, 0.13) m: $v = 0 \rightarrow \frac{\partial P}{\partial y} = 0$ (3.7a)

B.C at right upper edge, (x,y) = (0.12-0.30, 0.18) m: $v = 0 \rightarrow \frac{\partial P}{\partial y} = 0$ (3.7b)

B.C at right lower edge, (x,y) = (0.12-0.30, 0.05) m: $v = 0 \rightarrow \frac{\partial P}{\partial y} = 0$ (3.7c)

B.C at mid upper edge, (x,y) = (0.12, 0.13-0.18) m: $u = 0 \rightarrow \frac{\partial P}{\partial x} = 0$ (3.7d)

B.C at mid lower edge, (x,y) = (0.12, 0.00-0.05) m: $u = 0 \rightarrow \frac{\partial P}{\partial x} = 0$ (3.7e)

B.C at injection line, (x,y) = (0.3, 0.05-0.18) m: $P = P_{in} = 96000\ Pa$ (3.7f)

B.C at ventilation line, (x,y) = (0.00, 0.00-0.13)

and (0.00-0.12, 0.00) m: $P = P_{vent} = 16000\ Pa$ (3.7g)

Notice that $\Delta P = P_{in} - P_{vent} = 80000\ kPa$ which is equivalent to experimental pressure differential. Eq. 3.8 is the discretizated form of the Eq. 3.5 using second order central finite differences. The unknown pressure at a central inner point C (shown with solid black circles) is computed in terms of four neighbor pressures at N, S, W and E (see Figure 3.30) in Eq. 3.9 for $h_x = h_y$.

$$K_{xx}\frac{P_W - 2P_C + P_E}{h_x^2} + K_{yy}\frac{P_N - 2P_C + P_S}{h_y^2} = 0 \quad (3.8)$$

$$P_C = \frac{K_{xx}}{2\left(K_{xx} + K_{yy}\right)}(P_W + P_E) + \frac{K_{yy}}{2\left(K_{xx} + K_{yy}\right)}(P_N + P_S) \quad (3.9)$$

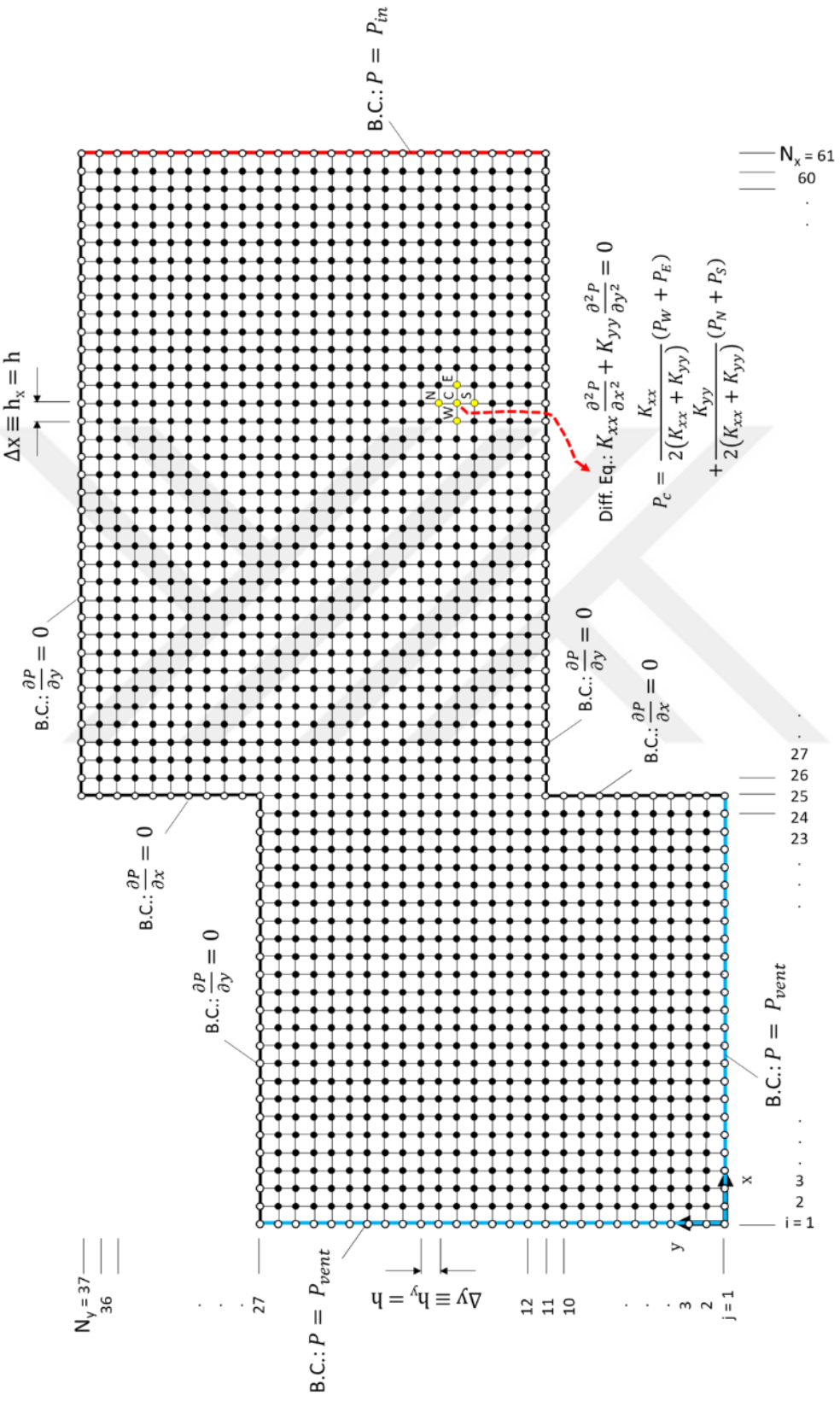

Figure 3.30: Discretized domain for the finite-difference method solution, governing differential equation for P along with boundary conditions.

The boundary conditions for the nodal points on the edges are computed using Equations (3.7a) – (3.7g). They are discretized using second order forward or backward finite differences as follows:

$$\frac{\partial P}{\partial y} = 0 = -\frac{1}{2h_y}\left(-3P_{1:25,27} + 4P_{1:25,26} - P_{1:25,25}\right)$$

$$\Rightarrow P_{1:25,27} = \frac{1}{3}\left(4P_{1:25,26} - P_{1:25,25}\right) \quad (3.10a)$$

$$\frac{\partial P}{\partial y} = 0 = -\frac{1}{2h_y}\left(-3P_{25:N_x,N_y} + 4P_{25:N_x,N_y-1} - P_{25:N_x,N_y-2}\right)$$

$$\Rightarrow P_{25:N_x,N_y} = \frac{1}{3}\left(4P_{25:N_x,N_y-1} - P_{25:N_x,N_y-2}\right) \quad (3.10b)$$

$$\frac{\partial P}{\partial y} = 0 = -\frac{1}{2h_y}\left(-3P_{25:N_x,11} + 4P_{25:N_x,12} - P_{25:N_x,13}\right)$$

$$\Rightarrow P_{25:N_x,11} = \frac{1}{3}\left(4P_{25:N_x,12} - P_{25:N_x,13}\right) \quad (3.10c)$$

$$\frac{\partial P}{\partial x} = 0 = -\frac{1}{2h_x}\left(-3P_{25,27:N_y} + 4P_{26,27:N_y} - P_{27,27:N_y}\right)$$

$$\Rightarrow P_{25,27:N_y} = \frac{1}{3}\left(4P_{26,27:N_y} - P_{27,27:N_y}\right) \quad (3.10d)$$

$$\frac{\partial P}{\partial x} = 0 = -\frac{1}{2h_x}\left(-3P_{25,1:11} + 4P_{24,1:11} - P_{23,1:11}\right)$$

$$\Rightarrow P_{25,1:11} = \frac{1}{3}\left(4P_{24,1:11} - P_{23,1:11}\right) \quad (3.10e)$$

While calculating the pressures at the corner points, (x,y) = (0.12, 0.05) m and (x,y) = (0.12, 0.13) m, as mentioned in [1], no-leakage through mold walls condition is considered: $\partial P/\partial n = 0$ where n is the normal outward vector to the mold wall. The corner points cause singularity. To resolve this problem, n is taken in the direction of 45° CCW with the positive y axis and 45° CCW with the negative y axis, for the corner points (x,y) = (0.12, 0.05) m and (x,y) = (0.12, 0.13) m, respectively and the corresponding second order finite differences can be written as follows:

$$P_{25,11} = \frac{1}{3}\left(4P_{24,12} - P_{23,13}\right) \quad (3.10f)$$

$$P_{25,27} = \frac{1}{3}\left(4P_{26,26} - P_{27,25}\right) \quad (3.10g)$$

Figure 3.31 shows the pressure distribution when the mold is filled completely with silicon oil and pressure and flow reached a steady state. Velocity components at each nodal point are calculated using Darcy's Law:

$$u = -\frac{K_{xx}}{\mu}\frac{\partial P}{\partial x} \tag{3.11a}$$

$$v = -\frac{K_{yy}}{\mu}\frac{\partial P}{\partial y} \tag{3.11b}$$

Pressure gradient components ($\partial P/\partial x \ and \ \partial P/\partial y$) are calculated using central finite differences for internal nodes and forward or backward finite differences for boundary nodes. Viscosity of the silicon oil, μ is taken as 0.106 Pa.s. Figure 3.32 shows the velocity distribution (quiver function of Matlab was used). Flow rates at the inlet and exit ports are calculated as $Q_{in} = 1.6587x10^{-7}\ m^3/s$ and $Q_{vent} = 1.6675x10^{-7}\ m^3/s$ using Eq. 3.12.

$$Q = \int_A |\boldsymbol{U}.\boldsymbol{n}\, dA| \tag{3.12}$$

where $\boldsymbol{U}$, $\boldsymbol{n}$ and A are the resin velocity, outward normal unit vector, and the inlet cross sectional area, respectively.

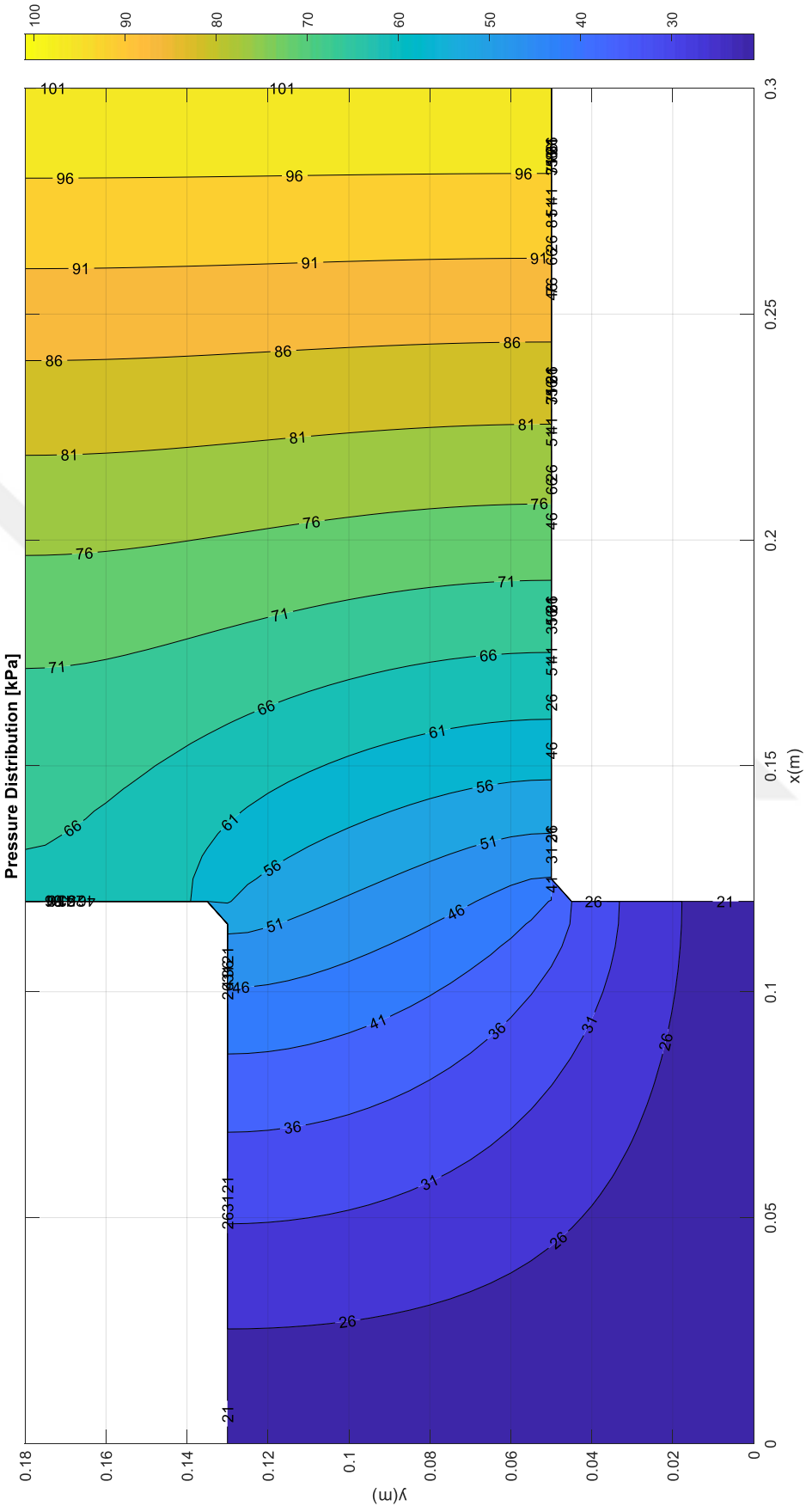

Figure 3.31: Pressure distribution at the end of mold filling.

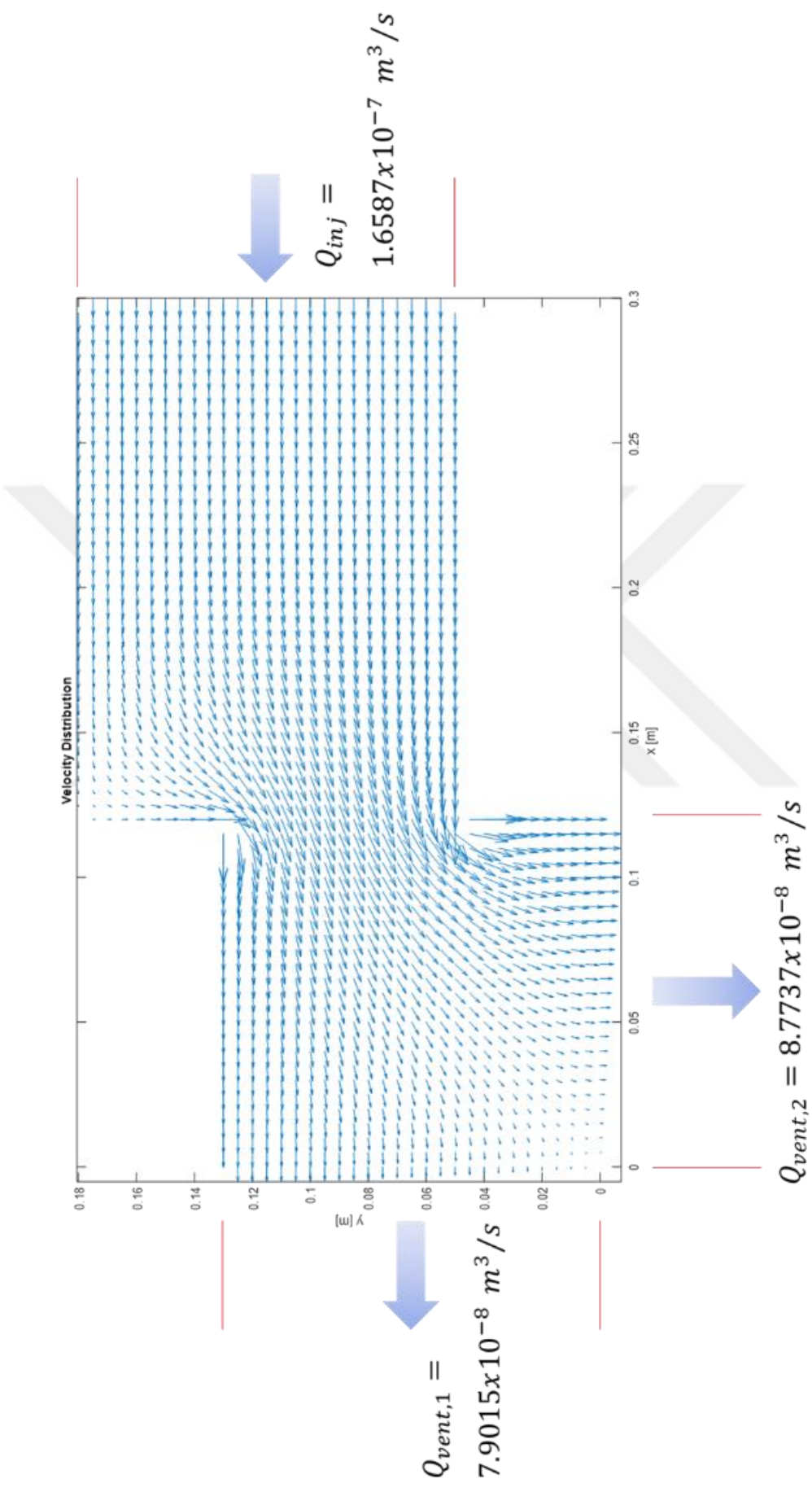

Figure 3.32: Velocity distribution in the mold.

Experimental resin mass at inlet is measured and recorded during resin infusion (see Figure 3.33). Curve fit is applied to the experimental mass versus time data for the last 60 seconds before injection is closed. Amount of resin mass flux entering the preform through the inlet is calculated as $1.6020x10^{-4}\,kg/s$. Mass flow rate in the model is calculated using $\dot{m} = \frac{dm}{dt} = Q_{in}\,\rho_{silicon\,oil}$ and found as $1.6106x10^{-4}\ kg/s$. When model and experimental mass flow rates are compared, they are almost same (and difference of 0.5%).

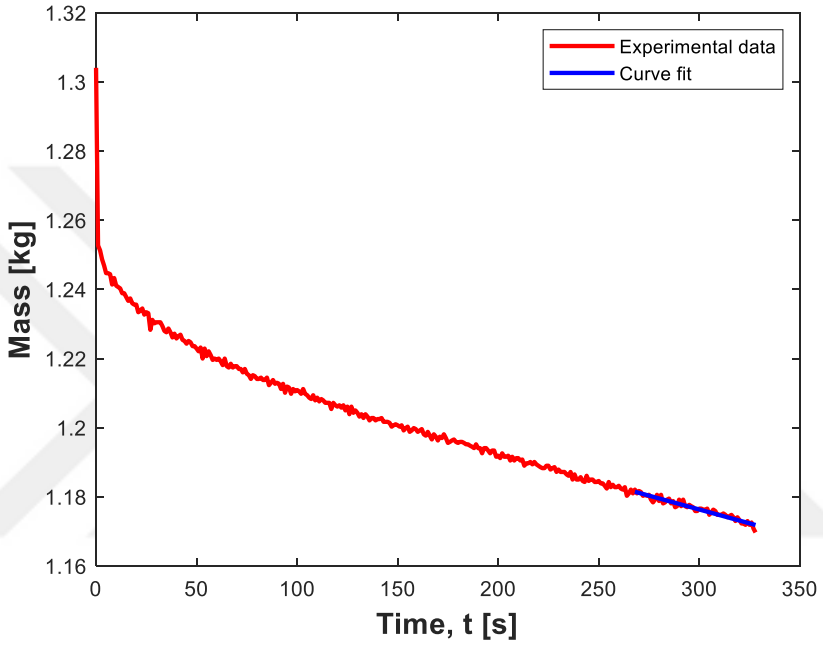

Figure 3.33: Mass of the silicon oil at the inlet during resin infusion.

In order to see the effect of resin bleeding, when the mold is filled with resin and the preform is assumed to be saturated completely, the injection gate is closed, and vacuuming is continued through the ventilation port. For 1D experiment, mean, standard deviation, maximum, minimum of 798 nodes (see blue regions in Figure 3.6) are calculated for the thickness distribution at five different instants (t = t_{fill}, t_{fill}+30 s, $t_{injclosed}$, $t_{injclosed}$+60 s and t_{end} = t_{600}).

At any time, t the maximum thickness variation between $h_{max}(x,y,t)$ and $h_{min}(x,y,t)$ is defined as

$$\Delta h_{variation} = h_{max}(x,y,t) - h_{min}(x,y,t) \tag{3.13}$$

and the corresponding variation in V_f is defined as

$$\Delta V_{f,variation} = \frac{n\,\rho_{sup}}{\rho_f}\left(\frac{1}{h_{min}(x,y,t)} - \frac{1}{h_{max}(x,y,t)}\right) \tag{3.14}$$

Thickness decreases from 1.95 +/- 0.38 mm (here 1.95 mm is the mean and 0.38 mm is the standard deviation of the thickness distribution) just before closing the inlet to 1.71 +/- 0.28 mm 300 s later. Corresponding fiber volume fraction, V_f increases from 17.4 +/- 3.1 % to 19.3 +/- 2.0 %, thickness variation (i.e., the difference between the maximum and minimum thickness values in the distribution decreases from 2.19 mm to 1.45 mm, respectively.

For 2D experiment, these calculations are done for 1064 nodes (see Figure 3.20, blue region) and seen that 1.72 mm is the mean and 0.27 mm is the standard deviation just before closing the inlet and 1.55 +/- 0.17 mm 300 s after closing. Thickness variation is 2.32 mm when injection is closed, and it is decreased to 1.55 mm and corresponding V_f increases from 19.4 +/- 3.0 % to 21.3 +/- 2.4 %.

For 1D model, maximum and minimum thicknesses are calculated using resin pressure data for 5 pressure sensor locations when just before the injection is closed. Calculated maximum (near inlet) and minimum (near exit) thicknesses of five sensors are 2.72 mm and 1.45 mm, respectively, and thus $\Delta h_{variation}$ is found as 1.27 mm and corresponding $\Delta V_{f,variation}$ is 11%. After 300 seconds when inlet is closed, thickness variation is reduced to 0.41 mm (maximum (near inlet) and minimum (near exit) are calculated as 1.83 mm and 1.42 mm, respectively) which corresponds to 5% V_f variation.

For 2D model, average, maximum and minimum thicknesses of 10 pressure sensors are calculated using power law formula $\left(V_f = C{P_c}^D\right)$ and using compaction pressure data (which is calculated using $P_c = P_{atm} - P_r$). Maximum and minimum thicknesses are 2.73 mm (near inlet, S04) and 1.25 mm (near exit, S10) just before closing the inlet and 1.69 mm (near inlet, S04) and 1.23 mm (near exit, S10) 300 s later, respectively. Thickness variation decreases from 1.48 mm (just before the inlet is closed) to 0.46 mm when inlet is closed and 300 s elapses which correspond to V_f variation from 14% to 7%, respectively. Detailed data is given in Table 3.2.

Table 3.2: Experimental and Model thickness and fiber volume fraction values at just before inlet is closed and 300 seconds later for resin bleeding (std stands for standard deviation).

		Experiment			
		1D		**2D**	
		Just before inlet closed	300 seconds later	Just before inlet closed	300 seconds later
$h\ [mm]$	mean	1.95	1.71	1.72	1.55
	std	0.38	0.18	0.27	0.17
	max	3.46	2.69	3.26	2.47
	min	1.27	1.24	0.95	0.91
$\Delta h_{variation}\ [mm]$		2.19	1.45	2.32	1.55
$V_f\ [\%]$	mean	17	19	19	21
	std	3	2	3	2
	max	26	26	34	36
	min	9	12	10	13
$\Delta V_{f,variation}[\%]$		16	14	24	22

Table 3.2: Continued

				Model				
				S04	**S05**	**S06**	**S07**	**S08**
1D	Just before inlet closed	$h\ [mm]$	upper	2.72	2.33	2.06	1.88	1.73
			mean	2.46	2.12	1.87	1.71	1.58
			lower	2.25	1.94	1.72	1.57	1.45
		V_f [%]	upper	14	17	19	21	23
			mean	13	15	17	19	21
			lower	12	14	16	17	19
	300 seconds later	$h\ [mm]$	upper	1.83	1.80	1.77	1.74	1.69
			mean	1.67	1.64	1.61	1.58	1.54
			lower	1.53	1.51	1.48	1.45	1.42
		V_f [%]	upper	21	22	22	22	23
			mean	20	20	20	21	21
			lower	18	18	18	19	19

Table 3.2: Continued

				Model									
				S01	**S02**	**S03**	**S04**	**S05**	**S06**	**S07**	**S08**	**S09**	**S10**
2D	Just before inlet closed	$h\ [mm]$	upper	2.66	2.27	2.07	2.73	2.25	1.93	1.71	1.59	1.62	1.57
			mean	2.35	2.01	1.83	2.41	1.99	1.71	1.51	1.40	1.43	1.39
			lower	2.11	1.80	1.64	2.16	1.78	1.53	1.36	1.26	1.29	1.25
		V_f [%]	upper	15	18	20	15	18	21	24	26	25	26
			mean	14	16	18	14	16	19	22	23	23	32
			lower	12	14	16	12	14	17	19	21	20	21
	300 seconds later	$h\ [mm]$	upper	1.69	1.67	165	1.69	1.67	1.63	1.59	1.56	1.56	1.55
			mean	1.49	1.47	1.46	1.50	1.48	1.45	1.41	1.38	1.38	1.37
			lower	1.34	1.32	1.31	1.35	1.33	1.30	1.26	1.24	1.24	1.23
		V_f [%]	upper	24	25	25	24	25	25	26	26	26	27
			mean	22	22	22	22	22	23	23	24	24	24
			lower	19	20	20	19	20	20	21	21	21	21

Chapter 4:

SUMMARY AND CONCLUSION

In this thesis, Structured Light Scanning (SLS) system is used for thickness monitoring of a composite material as it is being manufactured. It allows full-field thickness monitoring of an object (in this case, the composite part being manufactured, or compaction characterized) and SLS does not touch the object surface and thus does not disturb the part being measured. This system is successfully used for two different purposes: during compaction characterization and mold-filling and also post-filling experiments (for both 1D and 2D).

As the purpose of this thesis was not manufacturing actual composite parts but demonstrating the use of SLS thickness measurement system for both compaction characterization and real-time thickness monitoring during mold filling. Instead of actual materials, dummy materials (core material as reinforcement material and silicon oil as polymeric resin) are used in this study.

Compaction characterization experiments are conducted with a stack of 1, 2, 3, and 4 layers of core materials to relate a material's compaction behavior, that means how its thickness and thus fiber volume fraction, V_f changes as the compaction pressure, P_c acting on it changes. Thickness increases as the number of layers increases. However, because of the inversely proportional relationship between thickness, h and fiber volume fraction, V_f $\left(h = \frac{n\,\rho_{sup}}{\rho_f\,V_f}\right)$, V_f is not expected to vary among specimens made of different number of layers. However, literature has previous studies showing that the compaction level is not uniform in the through-thickness direction (more compacted near the contact surfaces than near the center of the specimen). Also, nonuniform fiber nesting may contribute to deviation from theoretically expected relationship between h and V_f, especially for some fabric types in which fibers or fiber bundles may find position in adjacent layers' empty spaces and thus thickness of the multiple layer specimen is further reduced. By using the dummy fabric in this study, typical fiber nesting issue of LCM processes is eliminated due to fabrication structure of the core material. Core material shows viscoelastic compaction behavior, meaning that when compaction pressure is kept constant, part thickness varies with time. Rate of thickness change (dh/dP_c) is higher at low compaction pressures than at high pressures.

During mold-filling experiments, resin pressure is recorded using pressure sensors and it is measured at five locations for 1D flow, and ten locations for 2D mold-filling experiments. Experimental thickness distribution is measured using SLS system. The modeling is achieved using experimental resin pressure data as the input. The resin pressure is recorded during experiments and compaction pressure, P_c is calculated using $P_c = P_{atm} - P_r$ formula. Fiber volume fraction, V_f is calculated by using a previously characterized relationship: power law formula $\left(V_f = C{P_c}^D\right)$ and modal constants (C and D) found with least-square method. Unsaturated (K_{uns}) and saturated (K_s) permeabilities in 1D mold-filling experiment is calculated as $2.96x10^{-10}$ m^2 and $2.93x10^{-10}$ m^2, respectively. An important note is that the permeability measurements are based on the assumption that the part thickness is constant; however here in this study it is not constant as the upper mold part is a flexible vacuum bag in VARTM process. So, average thickness is used in the computations as similarly done in Hancioglu's recent study [15] showing that the deviation is reasonably accepted. Unsaturated permeability, K_{uns} is calculated using flow front position versus time graph. Average thickness at 80 kPa compaction pressure (to calculate theoretical V_f) is taken as the average of last ten scanned thickness data within 300 seconds just before resin infusion (see *Permeability Characterization* in Chapter 3). The average thickness used in K_s calculation is taken as the average of last 60 seconds of before injection is closed. In 2D mold-filling experiment, pressure and velocity distribution at the end of mold-filling are simulated. The differential equation is derived by substituting Darcy velocity components in the mass conservation equation, and the boundary conditions are two types: no leakage along the mold wall, and resin pressure is known at the inlet and exit gates. Resin pressure is solved by discretizing the differential equation using Finite Difference Method (FDM) and solving the nodal pressures using iterative Gauss-Seidal method. At the steady state, flow rates at the inlet and vent are calculated as $Q_{in} = 1.6587x10^{-7}\ m^3/s$ and $Q_{vent} = 1.6675x10^{-7}\ m^3/s$, respectively. During mold filling experiments, mass of the silicon oil tank is recorded with time. When the mass versus time data is processed, the corresponding experimental volumetric flow rate at the inlet is calculated as $1.6498x10^{-7}\ m^3/s$. Thus the deviation of the model from the experiment is only 0.5% (= $(1.6587x10^{-7} - 1.6498x10^{-7})/\ 1.6587x10^{-7} * 100$).

As a further work, a fully automated and more accurate system for thickness monitoring and higher number and more accurate pressure sensors should be used. Also,

instead of small parts, larger parts such as used aerospace and automotive industries should be manufactured, preferably using the actual materials (fabric and resin).

BIBLIOGRAPHY

[1] S. G. Advani and E. M. Sozer, *Process modeling in composites manufacturing, second edition*. 2010.

[2] A. Wilson, "Vehicle weight is the key driver for automotive composites," *Reinf. Plast.*, vol. 61, no. 2, pp. 100–102, 2017, doi: 10.1016/j.repl.2015.10.002.

[3] M. Akif Yalcinkaya and E. M. Sozer, "Effect of part thickness variation on the mold filling time in vacuum infusion process," *J. Reinf. Plast. Compos.*, vol. 33, no. 23, pp. 2136–2150, 2014, doi: 10.1177/0731684414554938.

[4] B. Yenilmez and E. M. Sozer, "Compaction of e-glass fabric preforms in the Vacuum Infusion Process, A: Characterization experiments," *Compos. Part A Appl. Sci. Manuf.*, vol. 40, no. 4, pp. 499–510, 2009, doi: 10.1016/j.compositesa.2009.01.016.

[5] J. Li, "Modeling, design and control of vacuum assisted resin transfer molding (vartm) for thickness variation reduction," *Vacuum*, p. 181, 2006.

[6] T. Akyol, "Minimizing Thickness Variation in the Vacuum Infusion (VI) Process with 1D and 2D Resin Flows," 2012.

[7] S. P. McPherron, T. Gernat, and J. J. Hublin, "Structured light scanning for high-resolution documentation of in situ archaeological finds," *J. Archaeol. Sci.*, vol. 36, no. 1, pp. 19–24, 2009, doi: 10.1016/j.jas.2008.06.028.

[8] M. Ebrahim, "3D Laser Scanners: History, Applications and Future," *L. LAMBERT Acad. Publ.*, no. October, p. 104, 2016, doi: 10.13140/2.1.3331.3284.

[9] B. Caglar, B. Yenilmez, and E. M. Sozer, "Modeling of post-filling stage in vacuum infusion using compaction characterization," *J. Compos. Mater.*, vol. 49, no. 16, pp. 1947–1960, 2015, doi: 10.1177/0021998314541305.

[10] D. Modi, N. Correia, M. Johnson, A. Long, C. Rudd, and F. Robitaille, "Active control of the vacuum infusion process," *Compos. Part A Appl. Sci. Manuf.*, vol. 38, no. 5, pp. 1271–1287, 2007, doi: 10.1016/j.compositesa.2006.11.012.

[11] B. Yenilmez, "Vacuum Infusion (VI) process modeling and material characterization with viscoelastic compaction models," 2014.

[12] B. Yenilmez, B. Caglar, and E. M. Sozer, "Viscoelastic modeling of fiber preform compaction in vacuum infusion process," *J. Compos. Mater.*, vol. 51, no. 30, pp. 4189–4203, 2017, doi: 10.1177/0021998317699983.

[13] M. A. Yalcinkaya, B. Caglar, and E. M. Sozer, "Effect of permeability characterization at different boundary and flow conditions on vacuum infusion process modeling," *J. Reinf. Plast. Compos.*, vol. 36, no. 7, pp. 491–504, 2017, doi: 10.1177/0731684416684211.

[14] M. A. Yalcinkaya, A. Sarioglu, and E. M. Sozer, "A novel mold design for one-continuous permeability measurement of fiber preforms," *J. Reinf. Plast. Compos.*, vol. 34, no. 11, pp. 915–930, 2015, doi: 10.1177/0731684415581630.

[15] M. Hancioglu, E. M. Sozer, and S. G. Advani, "Comparison of in-plane resin transfer molding and vacuum-assisted resin transfer molding ' effective '

permeabilities based on mold filling experiments and simulations," 2020, doi: 10.1177/0731684419868015.

[16] HP 3D Structured Light Scanner. (n.d.). Retrieved from hp Web site: https://www8.hp.com/us/en/campaign/3Dscanner/overview.html

[17] 4 Reasons Why Composites are Replacing Traditional Materials. (2018). Retrieved from 3D Fortify: https://3dfortify.com/composites-replace-traditional-materials/

[18] Baris Caglar, "Experimental and Numerical Investigation of Material Characterization and Flow Monitoring in Liquid Composite Molding Processes," *PhD. Thesis, Koc University, March* 2017.

[19] D. Beach, C. Milroy, M. Kohn, and D. Somen, "David SLS-2 Tutorial," *Stanford Prod.* Realis. Lab, pp. 1–17, 2015, [Online]. Available: http://www.david-3d.com/en/products/sls-2.

Appendix A:

DAVID software interface for used SLS system.

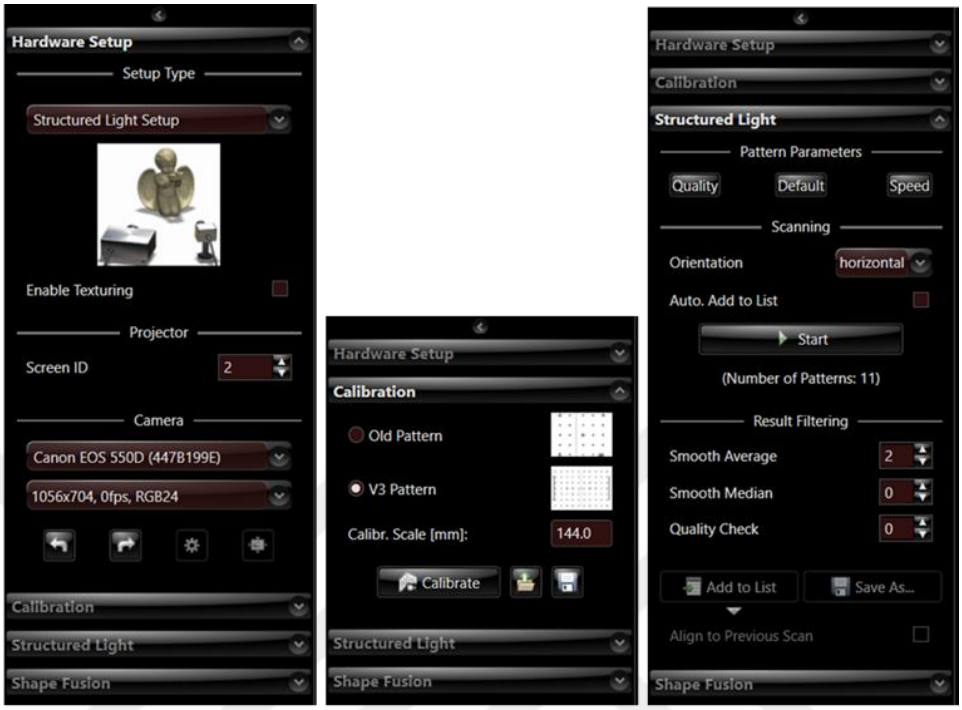

Figure A DAVID software: (a) Hardware Setup section, (b) Calibration section, (c) Structured Light section.

Appendix B:

Vacuum pressure regulator specifications.

■ **Stepless control of vacuum pressure in proportion to an electric signal**

Straight type Right angle type

Piping/Wiring Diagram

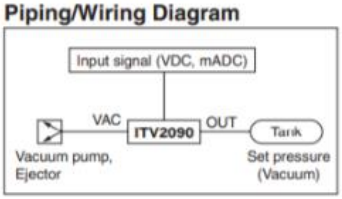

Standard Specifications

Model		ITV2090	ITV2091
Power supply	Voltage	24 VDC ±10%	12 to 15 VDC
	Current consumption	Power supply voltage 24 VDC type: 0.12 A or less Power supply voltage 12 to 15 VDC type: 0.18 A or less	
Minimum supply vacuum pressure (1)		Set pressure –13.3 kPa	
Maximum supply vacuum pressure		–101 kPa	
Regulating pressure range		–1.3 to –80 kPa	
Input signal	Current type (2)	4 to 20 mA, 0 to 20 mA	
	Voltage type	0 to 5 VDC, 0 to 10 VDC	
	Preset input	4 points	
Input impedance	Current type	250 Ω or less	
	Voltage type	Approximately 6.5 kΩ	
	Preset input	Approximately 2.7 kΩ	
Output signal (3) (Monitor output)	Analog output	1 to 5 VDC (Load impedance: 1 kΩ or more) 4 to 20 mA (Sink type) (Load impedance: 250 Ω or less)	
	Switch output	NPN open collector output: Max. 30 V, 30 mA PNP open collector output: Max. 30 mA	
Linearity		Within ±1% (Full span)	
Hysteresis		Within 0.5% (Full span)	
Repeatability		Within ±0.5% (Full span)	
Sensitivity		Within 0.2% (Full span)	
Temperature characteristics		Within ±0.12% (Full span)/°C	
Output pressure display	Accuracy	±3% (Full span)	
	Units	kPa (4) Minimum display: 1	
Ambient and fluid temperature		0 to 50°C (With no condensation)	
Enclosure		IP65 equivalent	
Weight		350 g	

Note 1) The minimum supply vacuum pressure should be 13.3 kPa less than the maximum vacuum pressure setting value.
Note 2) 4 to 20 mA is not possible with the 2-wire type. Power supply voltage (24 VDC or 12 to 15 VDC) is required.
Note 3) Either analog output or switch output must be selected. Furthermore, when switch output is selected, either NPN output or PNP output must also be selected. Use caution that the preset input type is not equipped with an output signal function.
Note 4) Please contact SMC regarding indication with other units of pressure.

Pc [kPa]	Accuracy [±3%]	Min - Max	Read on regulator during experiments [kPa]
2	0.06	2 – 2	2
5	0.15	5 – 5	5
10	0.30	10 – 10	10
20	0.60	19 – 21	19
40	1.20	39 – 41	39
60	1.80	58 – 62	59
80	2.40	78 – 82	78

Appendix C:

Thickness change in different chosen area for compaction characterization.

This figure shows the 1, 2, 3, and 4 layer core materials' thicknesses at different compaction pressures and areas. In compaction characterization experiments, whole specimen area is 200x100 mm^2 (41x21 nodes) and seen that there is no significant difference between an area of 20x20 mm^2 (5x5 nodes) and 45x45 mm^2 (10x10 nodes). As seen from the figure, standard deviation is higher at low compaction pressures when the chosen area is increased.

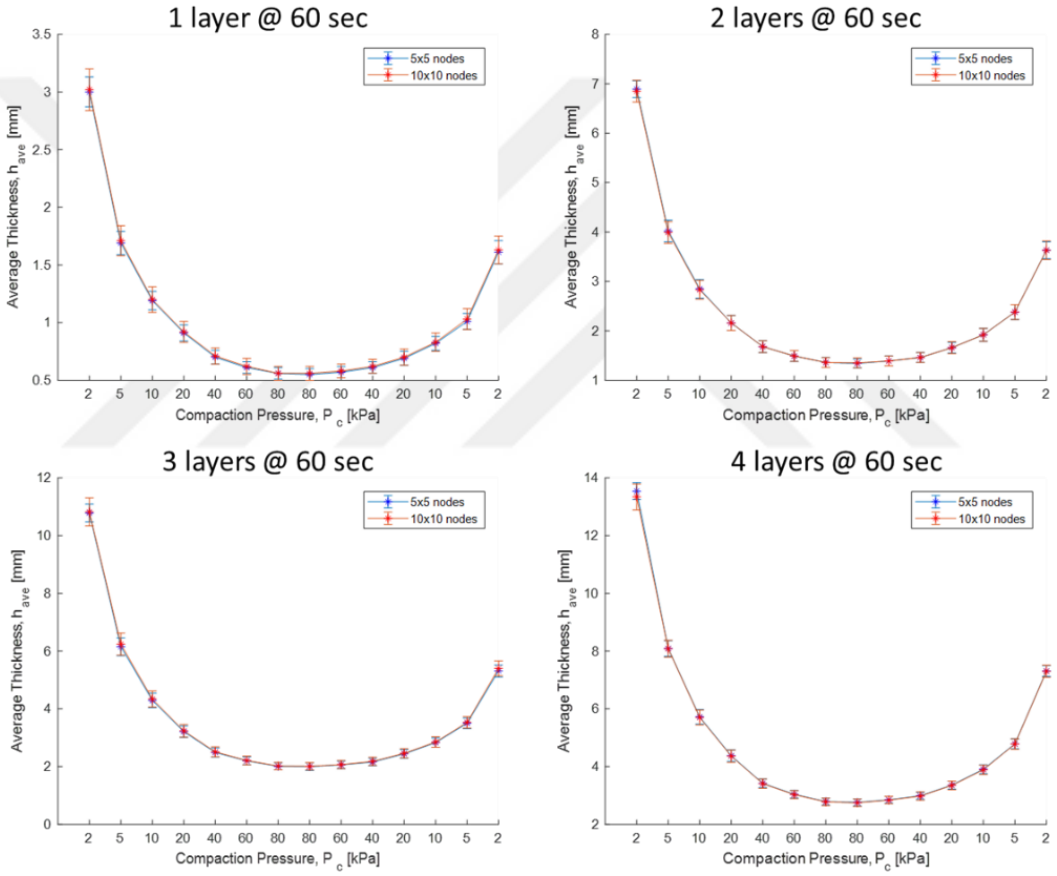

Figure C 5x5 and 10x10 chosen nodes comparison 1, 2, 3, and 4 layers at 60 seconds (different y-axis because of different layer numbers)